LTCC-BASED IMPEDANCE TUNER USING LIQUID METAL FOR
RECONFIGURABLE MICROWAVE CIRCUITS

by

INES AMOR

THESIS M. ENG. PRESENTED TO ÉCOLE DE TECHNOLOGIE
SUPÉRIEURE IN PARTIAL FULFILLMENT OF THE REQUIREMENTS
FOR THE DEGREE OF MASTER IN ELECTRICAL ENGINEERING WITH
THESIS
M. SC. A

MONTREAL, 12 OCTOBER 2021

ÉCOLE DE TECHNOLOGIE SUPÉRIEURE
UNIVERSITÉ DU QUÉBEC

BOARD OF EXAMINERS THESIS M.Sc.A.

THIS THESIS HAS BEEN EVALUATED

BY THE FOLLOWING BOARD OF EXAMINERS

Mr. Ammar Kouki, Thesis Supervisor
Department of electrical engineering at École de technologie supérieure

Mr. Sylvain G. Cloutier, President of the Board of Examiners
Department of electrical engineering at École de technologie supérieure

Mr. Andy Shih, Member of the jury
Department of electrical engineering at École de technologie supérieure

THIS THESIS WAS PRENSENTED AND DEFENDED

IN THE PRESENCE OF A BOARD OF EXAMINERS AND PUBLIC

ON OCTOBER 5TH, 2021

AT ÉCOLE DE TECHNOLOGIE SUPÉRIEURE

ACKNOWLEDGMENT

ADAPTATEUR D'IMPÉDANCE BASÉ SUR LA TECHNOLGIE LTCC UTILISANT LE MÉTAL LIQUIDE DÉDIÉ AUX CIRCUITS MICRO-ONDES RÉCONFIGURABLES
THESIS M.Sc.A.

Ines AMOR

RESUME

La reconfigurabilité dans le domaine de la RF/Micro-ondes est une tendance et un champ de développement en activité dans le cadre de la recherche scientifique vu l'évolution de la télécommunication et les systèmes sans fils ainsi que les appareils connectés dans notre vie quotidienne. Ces appareils nécessitent de plus en plus des composants fonctionnant en des hautes fréquences et sur des larges bandes. Ce qui fait appel à un besoin d'avoir technologie automatisée et reconfigurable permettant l'ajustement des paramètres afin de répondre aux spécifications exigées.

Dans ce contexte et vu l'importance des réseaux d'adaptation d'impédance dans la conception des circuits RF/Micro-ondes, nous avons développé nos idées dans le but de concevoir un tuner reconfigurable à base de métal liquide qui permet d'adapter des systèmes allant jusqu'à 10 GHz en fréquence. L'élaboration de ce tuner est basée sur la création d'une cellule à cavité.

La cellule résultante est établie, dans le fond, sur une ligne de transmission GCPW (grounded coplanar waveguide). Afin d'appuyer la notion de la reconfigurablilité, la cellule admet 2 états distincts; cavité vide (air) et cavité remplie avec un métal liquide. Cependant, le tuner est constitué par 8 cellules cascadées permettant la génération de 2^8 cas de comportement possibles.

Le développement du métal liquide nommé Galinstan, qui présente des caractéristiques non toxiques comparant à celles du Mercure utilisé auparavant, nous a permis de l'exploiter dans le cadre de notre projet et de découvrir les avantages et les inconvénients qu'il dispose. En outre, nous avons étudier la façon avec laquelle on peut le manipuler et le conserver.

Mots clés: réconfigurabilité, domaine de Radiofréquence/Micro-ondes, réseaux d'adaptation d'impédance, tuner fluidique et reconfigurable, ligne de transmission GCPW, métal liquide, Galinstan…

LTCC-BASED IMPEDANCE TUNER USING LIQUID METAL FOR RECONFIGURABLE MICROWAVE CIRCUITS
THESIS M.Sc.A.

Ines AMOR

ABSTRACT

Reconfigurability in Radiofrequency/Microwave domain is a trend and an active development field in the scientific research framework due to the evolution of the telecommunication and wireless system as well as connected devices in our daily life. These devices require more and more components operating at high frequencies with wide bands. Those requirements let us in need for an automated and reconfigurable technology that allows parameters adjustment in order to fit the needed specifications.

In this context, as the impedance matching networks are important for Radiofrequency/Microwave circuits design, we have developed our idea with the aim of designing a reconfigurable liquid metal tuner, which allows the matching up to 10 GHz in frequency. The development of this tuner is based on a cavity cell's design.

The resulting cell is implemented on a grounded coplanar waveguide transmission line. For the tuner reconfigurability, the cell admits 2 distinct states: empty cavity (air) and liquid metal-filled cavity. Therefore, the tuner is made up of 8 cascaded cells resulting the generation of 2^8 possible cases.

The development of the liquid metal called Galinstan, which exhibits non-toxic Characteristics comparing to Mercury characteristics used previously, has allowed us exploiting it within the framework of our project and discovering the advantages and drawbacks that it shows. In addition, we have studied the way to handle and package it.

Keywords: reconfigurability, Radiofreqency/Microwave domain, impedance matching networks, reconfigurable fluidic tuner, grounded coplanar waveguide transmission line, liquid metal, Galinstan

TABLE OF CONTENTS

LIST OF TABLES

LIST OF FIGURES

Page

LIST OF ABREVIATIONS

CMOS	Complementary Metal-Oxide-Semiconductor
DMTL	Distributed MEMS Transmission line
Freq	Frequency
GCPW	Grounded Coplanar Waveguide
HCl	Hydrochloric Acid
IPA	IsoPropyl Alcohol
LM	Liquid Metal
LTCC	Low Temperature Co-fired Ceramics
MEMS	MicroElectroMechanical System
NaOH	Sodium Hydroxide
Q-TEM	Quasi-Transverse ElectroMagnetic
RF	Radio Frequency
3D	Three Dimensions
Z_0	Characteristic Impedance

LIST OF SYMBOLS

β	Phase Constant of the Transmission Line
ε_{eff}	Effective Dielectric Constant
ε_r	Dielectric Constant
ε_0	Permittivity
Ω	Ohm
Γ_L	Load Reflection Coefficient
Γ_s	Source Reflection Coefficient

INTRODUCTION

Over the years, the number of wireless standards and applications has increased significantly leading to spectrum crowding and reduced spectrum availability. The RF circuitry needed to Thus, we need to use either multiple frequency or wideband frequency range systems. Multiple frequency systems need a huge RF front-end as they require a separated circuit for each frequency, where only one circuit could operate at once. Wideband frequency systems on the other hand may not offer optimal and consistent performance across different frequencies. Therefore, reusable and programmable RF and microwave systems can offer a good alternative that alleviates the limitations of the two mentioned approaches.

Compared to digital designs, RF and microwave designs are more complex and are very closely tied to the targeted hardware implementation. However, digital designs is generally based on functional description and implementation. Therefore, it does not require deep physical layer knowledge and it can be easily reconfigured. Hence, having a programmable RF system would bridge the gap between RF and digital design practices.

The programmable RF system is a group project composed by several sub-projects such as the vector RF measurements designed by Hana Mohamed in (Mohamed, H. 2019), the tunable MEMS/fluidic impedance tuners and control circuitry. Figure 0.1 illustrates a bloc diagram of the programmable RF system. Based on the measurement obtained using the reflectometer and the vector RF measurement bloc, the recognition system will calculate the source and the load reflection coefficients. Based on those results, the matching network control unit will extract the adequate configuration for the input and output matching networks.
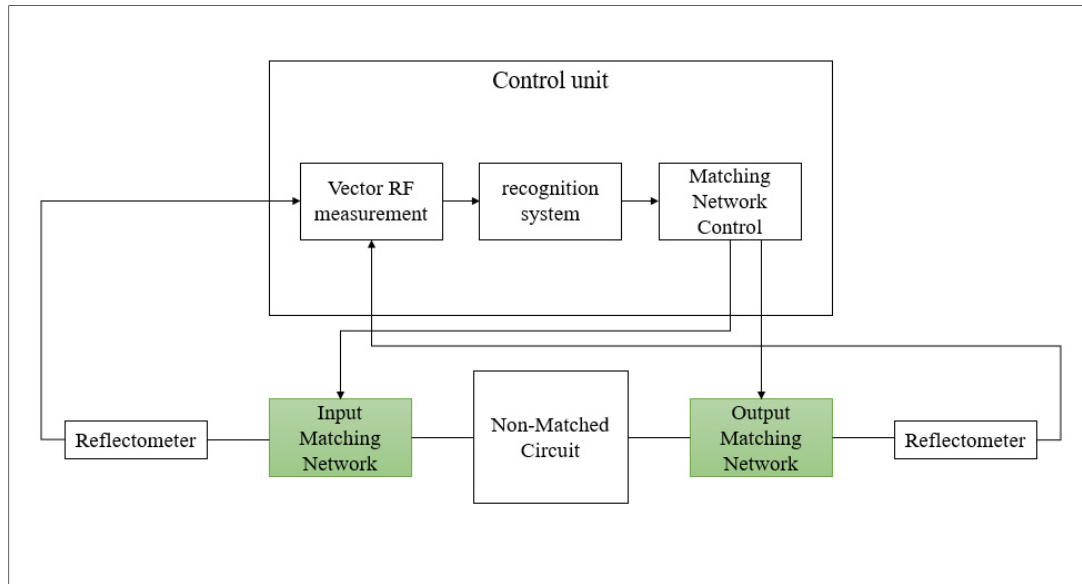
Figure 0. 1 Bloc diagram of the programmable RF system

In this context, we will focus on the design of reconfigurable tuner for impedance matching (green blocs in figure 0.1). However, there are several structures based on different technologies that can accomplish this. The available options will be studied in order to select the structure that fits to our requirements in terms of frequency and impedance coverage. These include MEMS-based tuners, dielectric fluidic tuners and liquid metal (LM) tuners. The liquid metal is one of the proposed solutions that is employed for reconfigurable RF circuits, especially for fluidic channels-based circuits on LTCC technology. For this reason, we are going to study the characteristics of some liquid metals, the way to handle a liquid metal and the impact of those metals on the RF behavior.

Research Problem

Since the matching network impedance is sensible to frequency variation, the problematic is to realize a reconfigurable impedance tuner that can provide adequate Smith chart coverage over the widest possible frequency band. Furthermore, we have to deal with the reusable circuit complexity in order to simplify the impedance tuner control.

Research Objective

The main objective of this thesis is to design, simulate and build a prototype of a reconfigurable impedance tuner using a LM structure. However, the LM oxidation can have an impact on the tuner's operation. For this reason, we have to revise LM handling and packaging methods.

The long term goal is to integrate the LM-based reconfigurable matching network in a programmable RF system. As it will be controlled by an automated control unit, we have to make the reusability of the prototype easy and study the reconfiguration repeatability, especially with the LM usage.

Contributions

The results obtained in this thesis are a subject of a letter paper entitled "Liquid Metal Investigation for LTCC-Based Reconfigurable Impedance Tuner", to be submitted for IEEE Microwave and Wireless Components Letters in October 2021. In this paper, we introduced the liquid metal-based RF circuits with implemented fluidic cavities. In addition, it summarized the design, simulation and prototype fabrication steps employed for LTCC technology and detailed some techniques used for liquid metal handling and packaging.

Thesis Organization

Chapter I presents a literature review focused on various impedance tuning techniques and technologies including the use of liquid metal.

Chapter II details the design modifications and the influence of the liquid metal employment on the design modeling and dimensions. It also sets forth the simulation results and the impact of the design variable on those results.

Chapter III presents the fabrication of the designed liquid metal tuner as well as a comparison of the simulated and measured results. It also discusses some fabrication challenges and the repeatability of measurements. The last chapter gives the main conclusions and recommendations for future work.

CHAPITRE 1

LITERATURE REVIEW

1.1　　　Introduction

This chapter provides the context and the background in which the present project has been carried out. It presents the basic concepts and theoretical foundation for the work and highlights the state of the art in the field of reconfigurable matching networks.

1.2　　　Impedance Matching: Fundamentals

Impedance matching, also sometimes called impedance tuning, consists of transforming the input or the output impedance of a non-matched device to a determined point (generally the reference impedance Zo, which is typically 50 Ω) in order to decrease the power reflection and/or maximize the transferred power. These two matching conditions become equivalent when the reference impedance for matching, Zo, is purely real. In addition to reducing the return loss, impedance matching can also reduce of the insertion losses (David M. Pozar, 1998). The matching circuits for a typical two-port device can be inserted as shown in the figure 1.1.
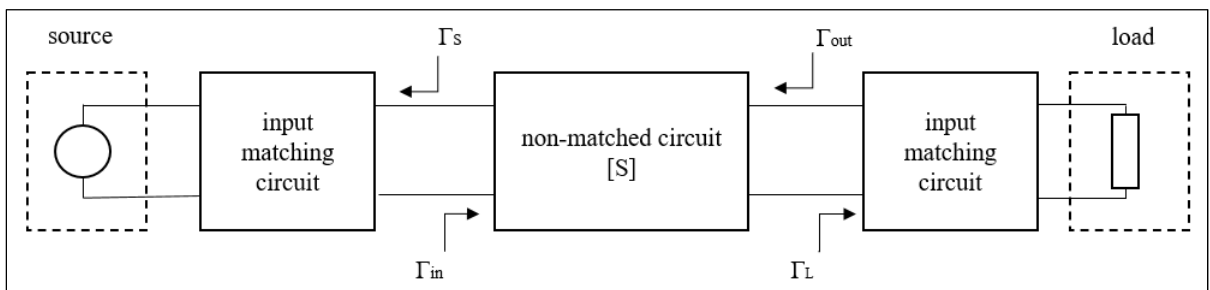
Figure 1.1 Bloc schematic of matched 2-port circuit

Under small signal operation, the non-matched device is characterized by its intrinsic S-parameters matrix (David M. Pozar, 1998). For a two-port device terminated by the reference

impedance Zo, S_{11} and S_{22} represent the reflection coefficients at the input and the output of the device, respectively. If the device is unilateral, i.e., $S_{12}=0$ or $S_{21}=0$, those coefficients are matched to the reference impedance otherwise the source and load reflection coefficients (Γ_S and Γ_L) are typically conjugately matched to input and output reflection coefficients (Γ_{in} and Γ_{out}) using the matching circuits. Ideally, matching circuits are composed of inductive and capacitive lumped elements to allow lossless impedance transformation from one value to another. However, it can become difficult to realize lumped components at high frequencies and one often resorts to distributed transmission line circuits, i.e., lines and stubs, for impedance matching.

According to (David M. Pozar, 1998), perfect matching is achieved when the reflection coefficient, Γ, at any given port of the circuit is equal to zero in the Zo reference system. On a logarithmic scale (in dB), this would correspond to minus infinity (-∞ dB) based on equation (1.1). In practice, perfect matching cannot be achieve and we have to fixe a dB value that established the acceptable matching level threshold. Figure 1.2 illustrates matching threshold levels of -20 dB (red circle) and -10 dB (blue circle) on the Smith chart with perfect matching representing the center of the chart. Points inside a given circle have better matching than threshold level. Therefore, to quantify the performance of matching networks, fixed or reconfigurable, we will assess their ability to transform impedances inside the circle that corresponds to the desired matching threshold level.

$$\Gamma_{dB} = 20\log|\Gamma| \tag{1.1}$$
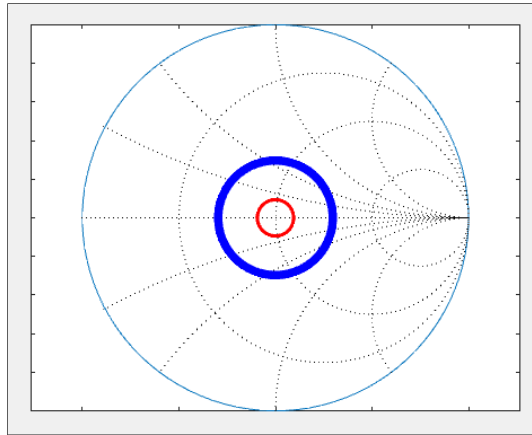
Figure 1.2 Illustration of the -20 dB and the -10 dB matching threshold levels

1.3   Reconfigurable Impedance Tuners

According to (Boeck, G. et al. 2003), RF front-end reconfigurable technologies are based on three different approaches. The first approach is the switching between two or more designed fixed networks. For each standard operating on a give frequency, one network is activated. The second approach uses a matching network made of multiple reusable blocs. It is also called mixed architecture. Some blocs are activated for all the frequencies while others are activated for specific ones. The third approach is the multifunctional blocs-based network in which the blocs can change their response during reconfiguration. This approach is categorized as a multi-standards architecture.

In addition to the different impedance tuner architectures, there exists different technologies for implementing their structures. These structures can be semiconductor-based, RF MEMS-based or fluidic channels-based.

1.3.1   Semiconductor-based Structures

The most common components for reconfigurable RF circuits based on semiconductor structure are the varactor and the PIN diode. The varactor can be defined as a diode with a

capacitive behavior, also called voltage-controlled capacitance, that can be employed for switching operations (Gaevski, M. et al. 2014). it is used for different reconfigurable components, particularly, for reconfigurable impedance matching networks. The PIN diode, on the other hand, acts like an RF resistance under forward bias and a capacitance under reverse bias. It is also used as a switcher (Boles, T. et al. 2011) and mostly employed for reconfigurable antennas (Nilolaou, S. et al. 2006).

In (Whatley, R. et al. 2006), the authors have developed a reconfigurable RF impedance tuner based on resonator sections as shown in figure 1.3. The resonators are made of microstrip loaded-lines and stubs. Both lines and stubs are loaded with varactors. The tuner operates at a center frequency equal to 5 GHz with a bandwidth between 1 and 2.2 GHz, depending on the load impedance.
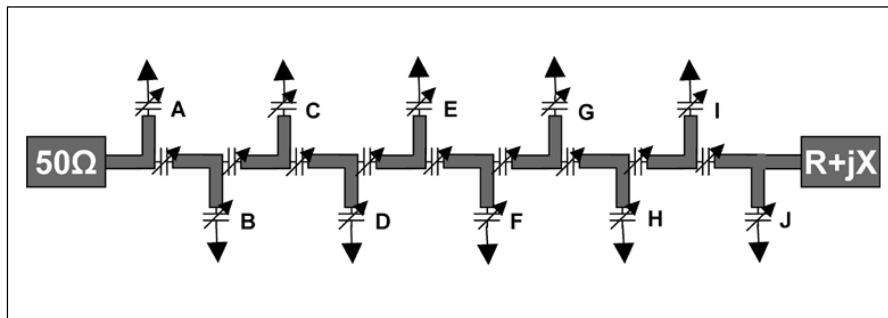
Figure 1.3 Resonator-based reconfigurable impedance tuner
Taken from Whatley, R. et al. (2006)

Another example of varactor-based tunable matching network was cited in (Buisman, K. et al. 2005). In this paper, the impedance matching tuner was designed for a single frequency (2 GHz) and implemented on Silicon-on-Glass technology. The paper focused on providing a low-distortion and low-loss tuner (less than 0.5 dB).

Semiconductor-based structures that use varactor and PIN diodes are generally used for a single frequency or a narrow frequency band, depending foremost of the load impedance. However, they tend to be lossy structures and cannot go high in frequency. In addition, the

capacitance variation during the reconfiguration can produce nonlinearity and distortion for RF signals (Buisman, K. et al. 2005). They also require biasing blocs with RF chokes for reconfiguration.

1.3.2   RF MEMS-Based Structures

RF MEMS structures (Rebeiz, G. M. 2006), mainly switches, offer good alternative to varactors and PIN diodes that provides very low loss behavior at high frequencies. RF MEMS switches can be in various architectures such as switching between pre-designed multiple matching networks or reconfiguring a single matching network.

An impedance tuner was designed in (Vaha-Heikkila, T. et al. 2006) based on single, double and triple-stub topologies using switched MEMS capacitors. It allows an acceptable coverage from 6 GHz frequency up to 20 GHz depending on the load impedance. The number of switches varies from 10 to 13 depending on the topology. An illustration of a single-stub impedance tuner with 10-switched MEMS capacitors is shown in the figure 1.4.
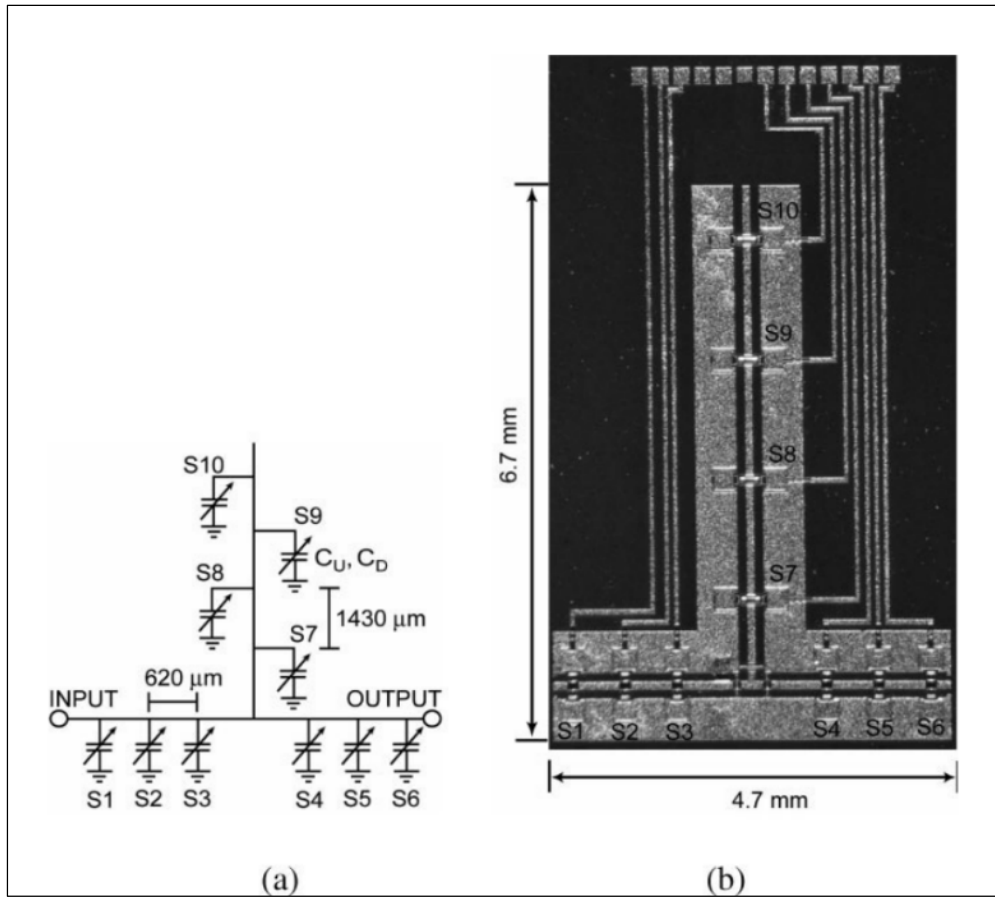
Figure 1.4 (a) circuit schematic and (b) microscopic illustration for single-stub
matching network using 10-switched MEMS capacitors
Taken from Vaha-Heikkila, T. et al. (2006)

Dual-beam MEMS switches was employed in (Domingue, F. et al. 2010) for a reconfigurable impedance matching network. The network was based on a slow-wave distributed MEMS transmission line for coverage improvement at low frequencies and tri-state capacitive MEMS switches for improving the bandwidth. The tuner operates from 5 GHz frequency and proves a good impedance coverage up to 20 GHz. This concept was developed in (Fouladi, S et al. 2012) where the MEMS was implemented on a CMOS chip to set forth the CMOS-MEMS technology. In addition, it was adjusted in order to fit a power amplifier design. The implementation of this network on the power amplifier allows it to operate from 3 GHz up to 7 GHz.

In genral, MEMS structures provide good impedance coverage at high frequencies and can be considered as almost lossless structures compared to varactor and PIN diode designs. Besides, they shows few drawbacks such as the contact resistance that depends of the surface contact. Moreover, the contact area can be damaged after a limited number of reconfigurations. They also need external electrical biasing though without an RF choke necessarily (Rebeiz Gabriel M. RF MEMS: Theory, Design and Technology book 2006).

1.3.3   Fluidic Channels-Based Structures

The fluidic tunable RF systems are reconfigurable systems based on the fluid movement and depending on the fluid characteristics. The fluid can be an insulator, i.e., water or a metal, i.e., liquid metal. By injecting or removing fluids around transmission line sections, the material properties can be altered locally resulting in changes in impedance and electric size. Hence, such structures can be used for impedance tuning and have been applied to the design of reconfigurable antennas, filters as well as power amplifiers.

In (Bao Jun Lei et al. 2012) the authors have designed a double stub liquid metal (LM)-based tuner. The concept of this design is to make the lengths of those stubs reconfigurable using LM. The same concept was later ameliorated by (Andy M. Morishita et al. 2015), where the tuner was implemented with a non-matched power amplifier as shown in figure 1.5. In this design, each designed stub is composed of 10 chambers with a length of 1.91 mm each. Thus, for each filled chamber; 1.91 mm length is added to the stub length. Therefore, 10^2 states are possible for each tuner. According to the paper, the tuner can be adjusted to operate in a frequency range starting from 3.37 GHz up to 6.02 GHz. Therefore, it allows the power amplifier to operate over a wideband.
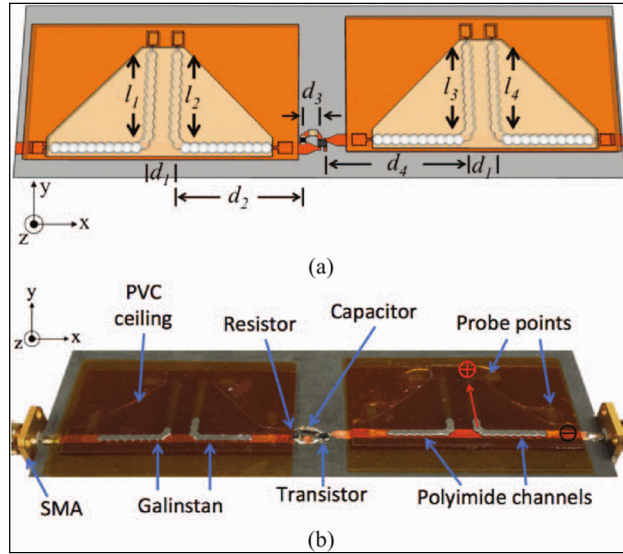
Figure 1.5 LM double stub tuner model
Taken from Andy M. Morishita et al. (2015)

The concept of fluidics is adequate also for cavity-based circuits in LTCC technology. In this context, a cavity-based tuner was developed in (Dorra Bahloul and Ammar B. Kouki 2020). The main idea of the paper is to design a cell that behaves as five transmission lines where one of them has a variable impedance. This cell is composed by a grounded coplanar waveguide (GCPW) built into an LTCC substrate with an implemented cavity on the top. Therefore, there are two states per cell. The first state is when the cavity is empty (air). The second state is when the cavity is filled with distilled water. The cascade of eight cells yileds 2^8 different impedances. The 3D illustration of a single cell of the tuner and its equivalent model are shown in the figure 1.6. In this figure, sections 1 and 5 (S1, S5) represent the tapered transitions that allow the on-wafer probe measurement while sections 2 and 4 (S2, S4) represent two GCPW (Grounded Coplanar Waveguide) interposed between two dielectric layers (thicknesses h_1 et h_2). These two sections present fixed parameters that depend on the design and the fabrication steps. The reconfigurability is provided by the section 3 (S3) which is the section covered by two dielectric layers. The first layer is cavity that can contain air or distilled water. The second layer is the LTCC dielectric layer. The advantage of this tuner is its ability to operate at low frequency 0.9 GHz to 2.4 GHz while providing adequate coverage of the Smith chart.

However, because of the dielectric loss of water at higher frequencies, this tuner is limited in frequency.
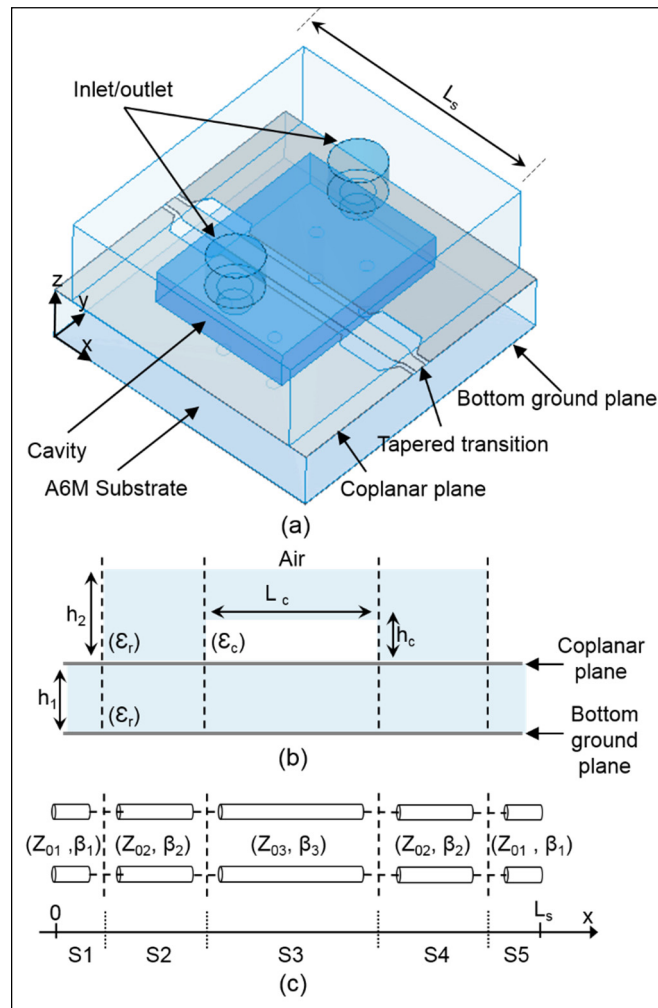
Figure 1.6 Fluidic cell's model
Taken from Bahloul, D. and B. Kouki, A. (2020)

1.3.4   Comparative Summary

As discussed in the previous sections, there are different approaches and technologies suitable for implementing reconfigurable impedance tuners with their respective advantages and disadvantages. Table 1.1 recapitulates the main characteristics of the different options.

Table 1.1 Comparative summary of various reconfigurable impedance tuner structures

Structure	Frequency coverage	Loss performance	Control method
Solid-state components	Low to medium	Moderate to high	Bias voltage (external bloc with RF choke)
RF MEMS	Medium to high	Very low	Bias voltage (external bloc w/o RF choke)
Microfluidic Channel	Variable: depends on the fluid characteristics	Moderate to high	Fluid mobility (injection and suction)

In the context of our project, we are going to design an impedance tuner based on fluidic cavities in an LTCC substrate, similarly to (Bahloul Dorra and Ammar B. Kouki 2020), but using liquid conductor (liquid metal LM) instead of a dielectric fluid. While liquid metals can offer advantages over dielectric fluids, their use comes with some challenges that must be taken into account.

1.4   Liquid Metal Handling Challenges

Different LMs have been used for implementing reconfigurablity of RF and microwave systems. The most well known LM in this field are the mercury (Hg), the eutectic gallium–indium binary alloy (EGaIn) and gallium–indium–tin ternary alloy (Galinstan). The Gallium-based alloys are classified as non-toxic liquid metals. However, mercury was recently excluded because of its toxicity (Gough, R. C. et al 2014). Table 1.2 summarizes the main LM characteristics.

Table 1.2 Liquid metals characteristics
Taken from Khondoker, M. A. H. and Sameoto, D. (2016) and Simon, J. (1997)

Liquid metal	Melting point (°'C)	Viscosity (cSt)	Conductivity (10^7 S.m^{-1})	Major Drawbacks
Mercury	-39	0.11	0.10	Toxicity
EGaIn	15.5	0.32	0.34	Oxidation
Galinstan	-19	0.37	0.38	Oxidation

The mercury LM is non-composed material. However, the EGaIn is composed of 75% Gallium and 25% Indium (Hayes, G. J. et al. 2012) while Galinstan is composed of 68.7% Gallium, 21.5% Indium and 10% Tin (Gough, R. C. et al 2014). According to (Cheng, S. and Wu, Z. 2012), the mercury shows a major drawback, other then the toxicity, which is the bead up inside the microfluidic channels. Considering the drawbacks of each solution, the mercury is eliminated from our study. Hence, we will focus on Gallium-based alloys.

Based on (L. Zhu and B. Wang 2020), the oxidation of the Gallium-based alloys is mainly caused by the Gallium composition. In order to minimize the oxidation impact, we have selected the LM that has less Gallium composition percentage. Comparing the EGaIn to the Galinstan, we have chosen the Galinstan LM for our project.

The use of LM requires that two main issues be addressed: (i) how to package and manipulate the LM safely while avoiding oxidation and (ii) how to inject it and extract it from the tuner.

1.4.1   Liquid Metal Packaging

The main issue of using Galinstan is its vulnerability to air or solid surface contact. According to (Liu Tingyi et al. 2012), the LM creates an oxidized skin and its color changes from skinny silver to dull gray as shown in the figure 1.7. One of the proposed solutions by the authors is to keep the LM in an environment where the level of oxygen is under 1ppm. This can be a

Nitrogen-filled box for example. Besides the complexity and the high cost of this solution, it is also uncertain; since we need to open the packaging box each time we use the LM.

Figure 1.7 Oxidation effect on a Galinstan droplet
Taken from Liu Tingyi et al. (2012)

(Morishita Andy M. et al. 2015) has also studied the LM oxidation issue. Their proposed technique was to immerse the LM into an electrolytic solution (HCI, NaOH). Therefore, the LM can be manipulated inside a HCI or NaOH-filled box. Noting that the electrolytic solutions are cheap, this packaging option can be considered as adequate for our requirements.

1.4.2   Liquid Metal Pumping Operation

The major drawback provoked by the oxidation is that the formed skin can leave residues in fluidic channels when trying to take off the injected material (Koo Chiwan et al. 2015). This make the repeatability of the pumping-cleaning operation more complicated. Consequently, the pumping operation can be considered as a critical step. An injection method was provided by (Koo Chiwan et al. 2015) using syringes as shown in figure 1.8. The authors have proposed the Distilled (DI) water as a carrier liquid for the LM injecting.
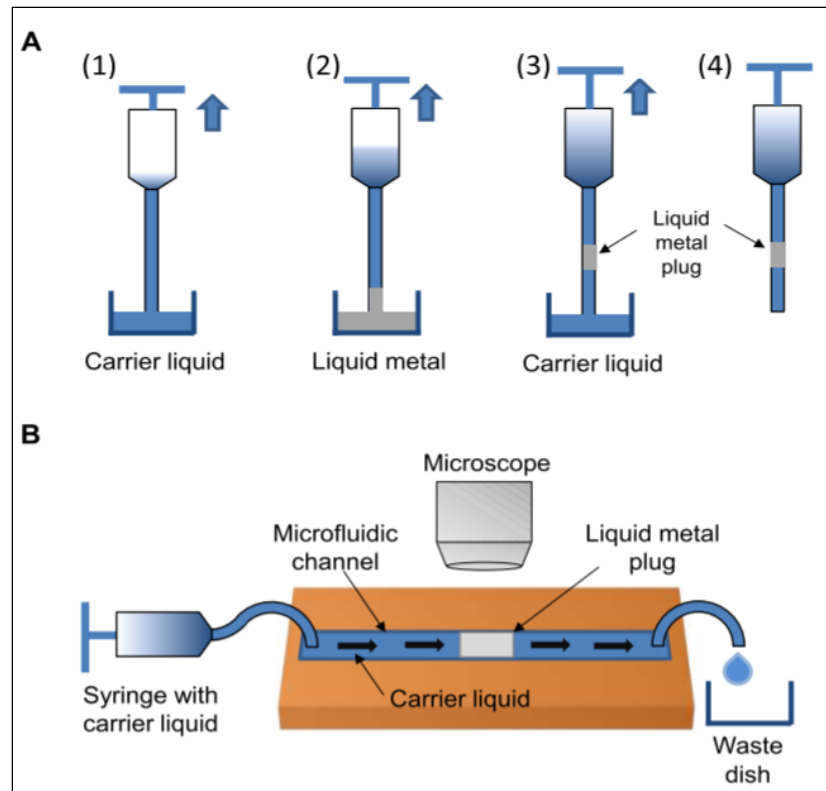
Figure 1.8 Injection of the LM in fluidic channels
Taken from Koo Chiwan et al. (2015)

The NaOH is a water-based electrolyte solution employed for LM manipulation in tunable systems and RF switches (Kareem S. Elassy et al. 2019). Despite its lossy behavior, it has been implemented in different RF components with electrical actuation as a carrier solution (Matthew R. Moorefield et al. 2018). However, it allows increasing the circuit losses as well as the RF performance.

To conclude, we have chosen the Galinstan LM for our project due to the advantages that it presents compared to the mercury and the EGaIn. In addition, we will develop a technique to facilitate the pumping-cleaning operation of Galistan using the NaOH given its ability to prevent the LM oxidation.

CHAPITRE 2

LIQUID METAL TUNER DESIGN AND SIMULATION

2.1   Introduction

The targeted LM tuner design is based on the recently proposed LTCC fluidic tuner (Dorra Bahloul and Ammar B. Kouki 2020). Therefore, we will consider the expected limitations and constraints of using LM instead DI water and take them into account in determining the required modifications to the tuner's design. We will then proceed with the design of the LM-based tuner using both an equivalent model representation and full-wave field simulation.

2.2   Fluidic Cells for Liquid Metal Operation

The major difficulties in using LM are its interaction with other materials, its fast oxidation and its physical characteristics, which can produce drawbacks during injection and pumping.

2.2.1   Liquid Metal's Interactions with Other Materials

According to (Zhu L. et al. 2020), the contact between LM and other materials, especially metals, can cause the changes in the other material's characteristics. For metals, these changes can affect the metal's conductivity. In some cases, the contact can also result in corrosion related to metal reactivity. The reaction caused by this contact may affect the device's reliability and robustness. Therefore, such contacts should be avoided in our tuner design. In our case, the original cavity of the fluidic cell is embedded directly on the transmission line and keeping it as is would result in a contact between the LM and the silver of the transmission line (see figure 2.1a). Therefore, we have separated the cavity and the transmission line with a thin dielectric layer as shown in the figure 2.1b to protect the silver from being attacked by the LM.
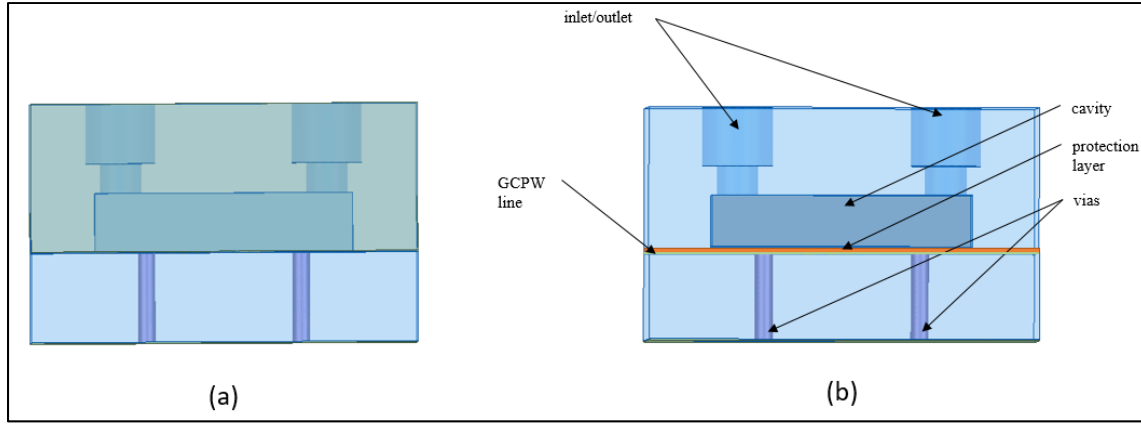
Figure 2.1 (a) original cell design (b) modified cell design

The operation and performance of the tuner is determined by the change in capacitance that can be achieved for the unit cell between its empty cavity state, low capacitance, and its LM filled stated, high capacitance. The bigger the ratio between these two states, the better will be the Smith chart coverage of the impedance tuner. For the LM filled state, the resulting structure formed by the transmission line and the bottom surface of the filled cavity separated by the dielectric protective layer can be modeled by a low-impedance transmission line whose per-unit length capacitance can be calculated using the well-known expression (Grove, T. T et al. 2005):

$$C = \frac{\varepsilon_0 \varepsilon_r A}{d} \tag{2.1}$$

where ε_0 is the permittivity of vacuum, ε_r is the dielectric constant of the protective layer, A is the plate area (cavity bottom surface) and d is the distance between the two plates (thickness of the protective layer). Therefore, to maximize performance the LM filled state capacitance must be maximized. Since the entire tuner is designed in DuPont 951 LTCC material, ε_r is fixed. Consequently, only the cavity's area, A, and the protective layer's thickness, d, remain as design variables. Keeping A fixed, we built a 3D model of a single cell and simulated it using HFSS for two different thicknesses corresponding to a single 2-mil (d=45.18um after shrinkage) and two 2-mil layers (d=86.36um after shrinkage). Figure 2.2 shows the obtained S_{11} between 1 GHz to 10 GHz where it can clearly be seen that the thinner protective layer yields a significantly better coverage in the Smith chart.
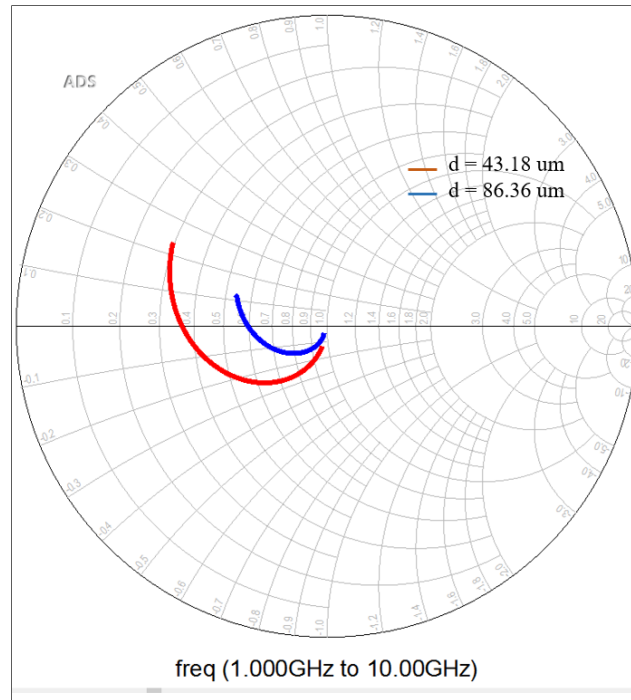
Figure 2.2 Single cell simulated S_{11} (a) d = 43.18 um (b) d = 86.36 um

The low impedance transmission line model of the LM-filled cell can be characterized by (2.2). In fact, increasing the dielectric layer thickness, will decrease the capacitance C. Which allows the characteristic impedance of the model to raise. Using two dielectric sheets (blue curve), the characteristic impedance, that presents the S_{11} rotation center, becomes closer to 50 Ω. Which results a reduced S_{11} movement on the Smith chart

$$Z_0 = \sqrt{\frac{L}{C}} \tag{2.2}$$

Where L and C are the inductive and the capacitive parts of the transmission line.

2.2.2 Liquid Metal's Fast Oxidation

2.2.2.1 Impact on Pumping Operation

As proved by other researchers, the LM shows a fast-spontaneous oxidation following oxygen attacks or even surface contact. Furthermore, this oxidation can cause characteristics changes that influence the cell's behavior. According to (L. Zhu and B. Wang 2020), the Gallium is the cause of the fast oxidation (see chapter I). The formed skin is indeed an oxide Gallium skin. However, its thickness is conserved and does not increase. This act is called the self-limiting effect. As a result, we can make sure that the LM do not solidify when injected inside the cavity. In addition, the LM viscosity is higher then water viscosity (2.4 mPa.s at 20 °C). Still to verify if the outlet dimensions are suitable for LM injection. A pumping-cleaning operation is needed to clear any doubts.

As an initial investigation, we have used an existing fluidic cell sample and injected the LM inside it in order to make sure that with the same outlet dimension we can fill the whole cavity. Figure 2.3 shows the results obtained using X-Ray imaging and demonstrates that the LM reached all of the cell's corners. Therefore, the outlet dimensions of the original fluidic cell can be conserved for LM use.
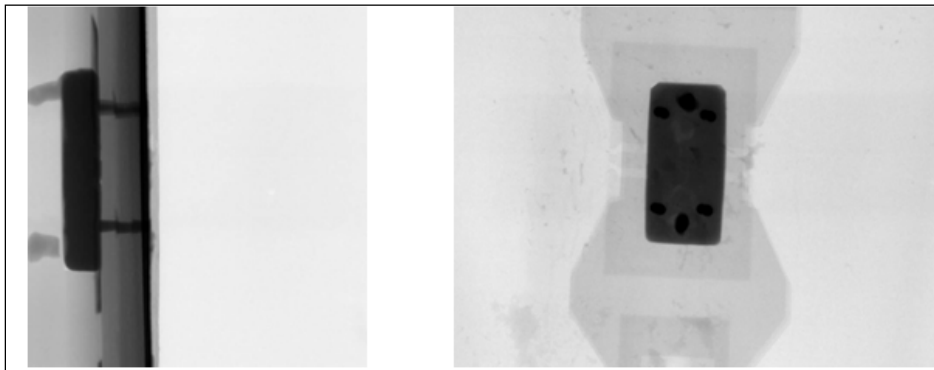

Figure 2.3 side view and top view of LM-filled cell

2.2.2.2 Impact on the Operating Behavior

The transformation of the LM from one state to another under oxidation produces changes in its physical and electrical characteristics. Those changes can affect the device's functioning. Therefore, we have to make sure that the cell will perform even with the LM oxides inside.

(Kim D. et al. 2013) proposed to handle the liquid metal into the fluidic channels using an HCl-impregnated paper inserted between the wafer and the channel to prevent the Galinstan from oxidation. It was proven that the proposed solution allows the LM to remained oxide-free and move inside the fluidic channels without sticking or leaving residues behind. (Kim D. et al. 2015) studied this solution and demonstrated that the operation took 60 min to be established. It means that after 60 min from injection, the Galinstan inside the fluidic channel becomes oxide-free. However, the HCl-impregnated paper effect lasts only 30 days and our interest is to find a permanent solution for the oxidation issue in order to guarantee the circuit reconfigurability. Fortunately, based on the research of (L. Zhu and B. Wang 2020), it was found that despite fast Gallium oxide skin development in Gallium-based alloys, the Gallium composition does not affect the LM-based circuit functionality. As a result, we can suppose that the performance of the cell will stay stable even with the appearance of the Gallium oxide skin.

As a conclusion, the Galinstan is an appropriate LM that is suitable for our targeted impedance tuner design. In spite of the difficulties in handling and maneuvering, it is still a useful material in fluidic devices thanks to its adequate characteristics for RF and microwave application.

2.3   Liquid Metal Cell Design

2.3.1   Liquid Metal Cell Modeling and Dimensioning

The equivalent model of the original fluidic cell is shown in figure 1.6. By analogy to this model, the LM-based cell is also divided to five sections where the third one is a variable

impedance transmission line, and the other sections are GCPW (Grounded Coplanar Waveguide) lines. Figure 2.4 illustrates a cross-section view of the designed LM cell and its proposed equivalent model. The presence of the protective dielectric layer can easily be seen in this figure.
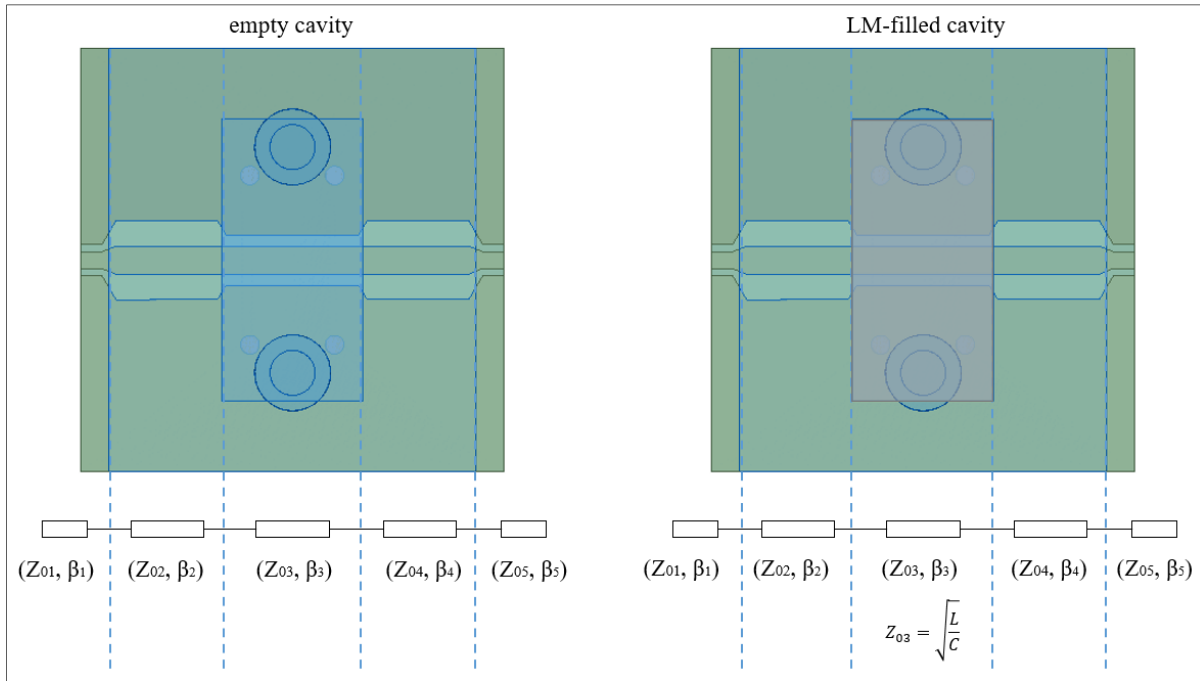
Figure 2.4 LM cell model

Sections 1, 2, 4 and 5 are characterized by their effective dielectric constants ε_{eff} and their characteristic impedances Z_0 and they are common between the dielectric and the LM configurations. According to (Dorra Bahloul and Ammar B. Kouki 2020), the S1 and S5, which are the tapered transition, are conventional GCPW line. Their characteristics are already accessible and can easily be calculated using software tools. For S2, S4 and S3 in the empty state, (Dorra Bahloul and Ammar B. Kouki 2020) have also employed the conformal mapping techniques for Quasi-Transverse ElectroMagnetic Q-TEM modes to establish closed-form expressions for the impedance and electric size used in the design (ANNEX I).

The empty cavity state was taken as a reference to calculate the GCPW dimensions (W and G) for each section with a 50 Ω characteristic impedance required. The dimensions are summarized in the table:

Table 2.1 GCPW sections' Dimensions
Taken from Dorra Bahloul and Ammar B.Kouki (2020)

Sections	S1 and S5	S2 and S4	S3
W (μm)	125	200	200
G (μm)	40	150	65

For the LM filled state, the section S3 is modelled by a low impedance transmission line formula, where the characteristic impedance can be approximately calculated using (2.2). However, the capacitive factor of the formula is the dominating part in our case. Therefore, we can conclude about the impact of the cavity area and the distance between the cavity and the GCPW line on the capacitance value. As the dimensions are already fixed, the capacitance value can be calculated (2.9). The dimensions are detailed in and yield a capacitance of 3.2 pF when the protective dielectric layer is 43.18 um thick.
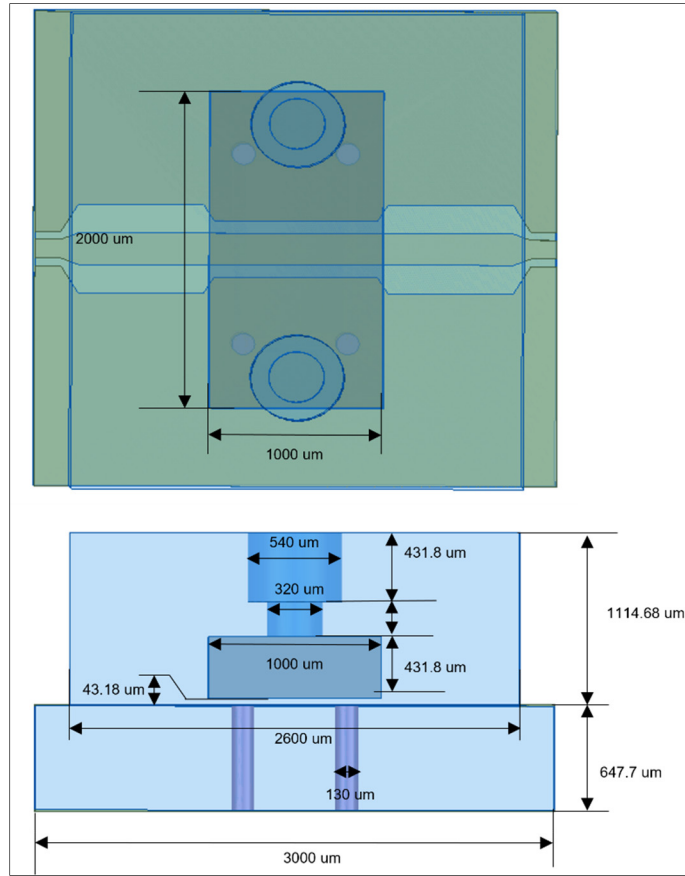
Figure 2.5 The cell's final dimensions

The design is composed of nine layers, where eight of them are 5 mil layer and one is 2 mil layer. The first, second and the third layer contain the vias in order to insure the connection between the ground plan and the metal. The metal is printed on the top of third layer. The forth layer is the metal protection layer and it is less thick then the others (2 mil). The upper layers contain the fillable cavity and the other cavity windows.

2.3.2   Liquid Metal Cell's Characteristics: Simulation Results

Since the cell acts like cascaded sections of transmission lines, we can use this approach to simulate the behavior of the cell for the two possible states (empty, filled). First, we simulate the reflection coefficient of the source (S_{11}) for each case from 1 GHz to 10 GHz. Figure 2.5 shows the results obtained using the HFSS 3D field simulator. As discussed in the previous

sections, a 50 Ω impedance is provided when the cavity is empty (red curve). On the other hand, we have obtained an impedance variation when the cavity is LM-filled (blue curve). The extent of the obtained variation in this simulation has a major impact on the tuner coverage. Therefore, the more this variation increases, the more impedances can be covered.
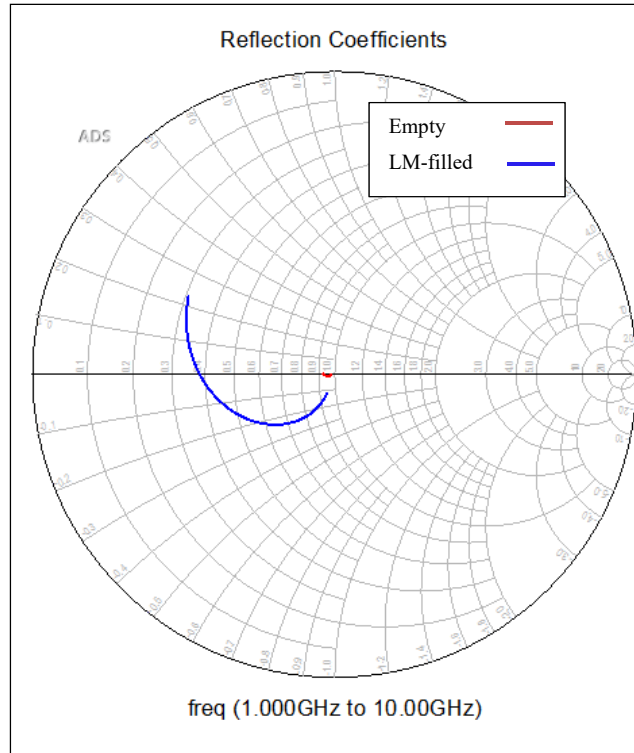
Figure 2.6 Simulated S_{11} of the cell for empty and LM-filled states

The cell's insertion loss (S_{21}) can also provide an idea about the difference between the empty and the LM filled behavior as shown in figure 2.6. We can notice that, for the empty cavity (red curve), we have less than 0.25 dB insertion loss up to 10 GHz. On the other hand, for the LM-filled cavity (blue curve), the insertion loss increases faster with frequency.
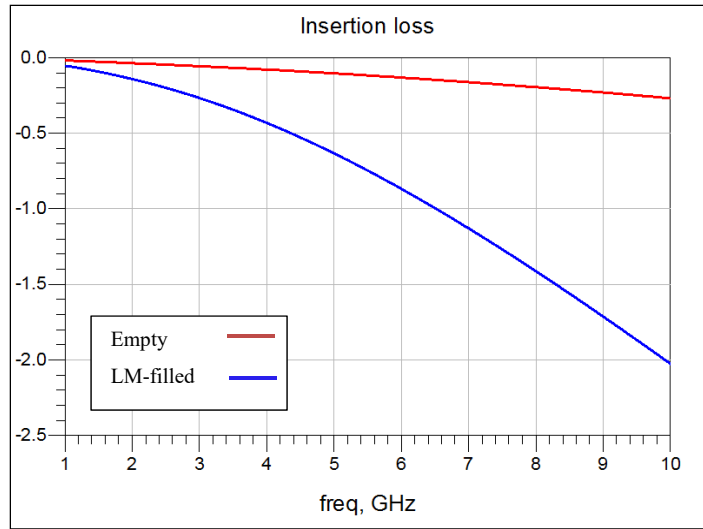
Figure 2.7 Simulated insertion loss of a single cell for empty and LM-filled states

2.4 Liquid Metal Impedance Tuner Design

The impedance tuner is composed of eight cascaded cells. Using the HFSS design of the single cell discussed previously, we have designed the whole tuner as shown in the figure 2.7 and where the entire tuner's response is obtained by cascading the S-parameters of the individual cells. For measurement purposes, transitions to SMA connectors have to be included.
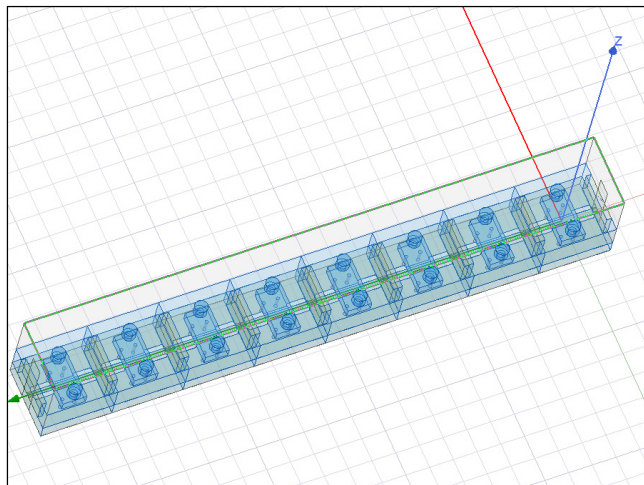
Figure 2.8 8-cell impedance tuner

2.4.1   SMA Transition Design and Simulation

Since the LM pumping operation is critical, we need to measure the tuner's characteristics while injecting the LM with a physically robust setup. Therefore, we use SMA connectors for both source and load sides instead of using on-wafer probes. Considering the SMA connector's dimensions, its integration requires two extra source and load transitions with suitable dimensions. Using ANSYS HFSS software, we designed the transitions shown in the figure 2.9.
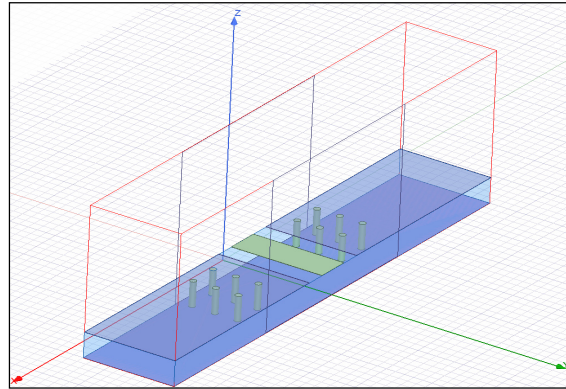
Figure 2.9 3D design of the transition

In order to retain the source and the load impedance, the GCPW line dimensions are calculated using Linecalc of ADS software to obtain a matched line as shown in the figure 2.10 (a red dot at the center of the Smith chart). The transition design and its inclusion in the simulations help to insure that simulation resulted are representative of the physical structure and its measured results.
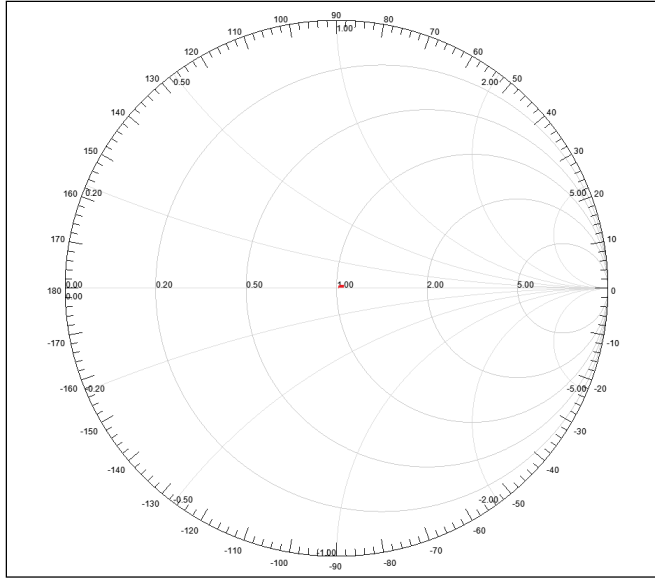
Figure 2.10 Simulated S_{11} of transition structure

2.4.2 Impedance Tuner: Simulation Results

As discussed, the tuner design is composed by cascaded cells with each cell having two possible states: empty, referred to as state '0', and LM-filled, referred to as state '1'. For n-cells, the tuner has 2^n possible states.

To simulate the tuner design, we exported the S-parameters data matrix of a unit cell for both states '0' and '1' from the ANSYS HFSS 3D field simulator. These were then imported into the Advanced Design System (ADS) software as shown in figure 2.11 for eight-cells (256 possible states).
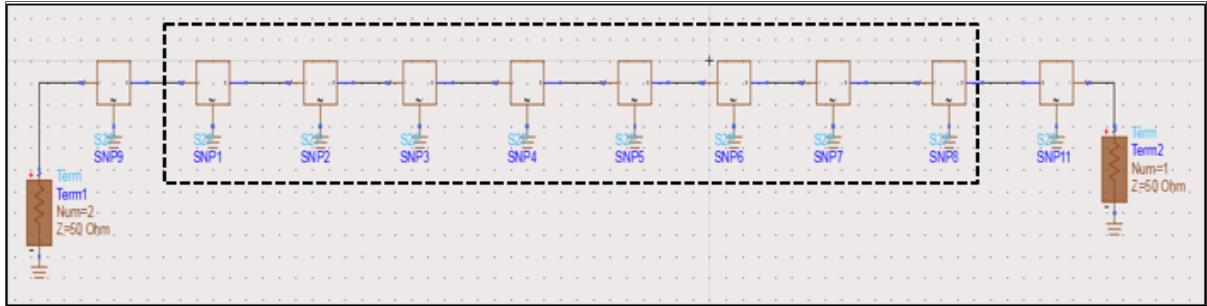
Figure 2.11 ADS illustration for the tuner's circuit
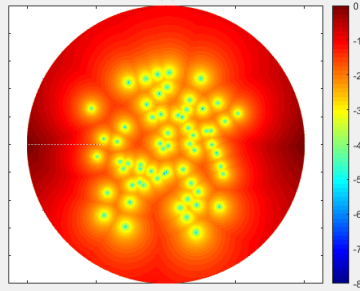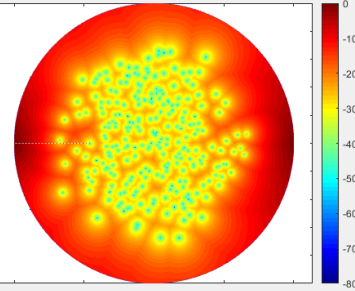
The tuner cells are surrounded by a dashed line. However, there are two extra S2P components on the source and the load sides. These components include the field-simulated S-parameters of transitions to SMA connectors as discussed in the previous section.

To assess the predicted performance of the impedance tuner, we first define a quantifiable coverage metric as the percentage of the Smith chart area that can be covered for a specific matching threshold, e.g., under -20dB or -10dB. For this simulation, we will consider the return loss performance simulated over the Γ plane as proposed and explained in (Domingue, F. 2008).
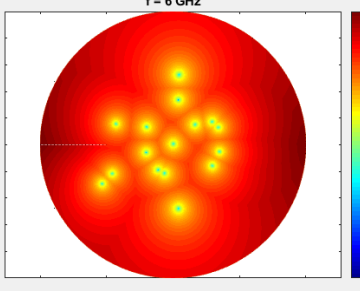
2.4.2.1 Coverage versus Number of Cells

The number of cells that make up the impedance tuner can be varied so that the smallest tuner, i.e., lowest number of cells with the acceptable coverage can be selected to reduce size, cost, complexity and loss. Therefore, our goal in this part is to study the impact of the number of cells on the impedance area that can be covered by the tuner. To this end, we developed a Matlab code that allows us to shade areas of the Smith chart based on the achievable S_{11} matching value for a given tuner setting. We then calculate the percentage of Smith chart coverage that the tuner can provide for the two chosen matching thresholds (-10dB and -20dB). Table 2.2 shows the obtained coverage for 4, 6 and 8-cell tuners at the center frequency 6 GHz.

Table 2.2 Coverage in function of the number of cells at 6 GHz

4 cells	6 cells	8 cells
16 points	64 points	256 points
C-10dB = 75.64 %	C-10dB = 87.70 %	C-10dB = 93.91 %
C-20dB = 30.10 %	C-20dB = 55.67 %	C-20dB = 71. 52%
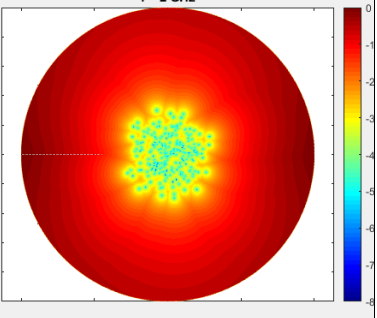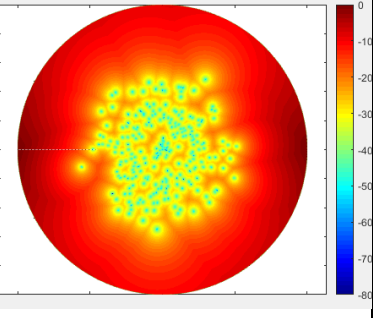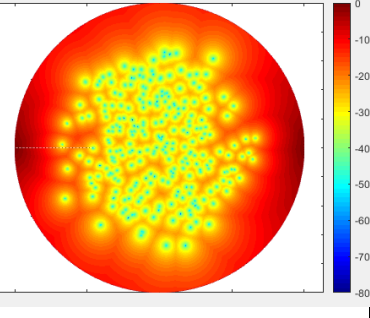
According to the table 2.2, the number of the cells can be minimized if the design does not require a high matching threshold. However, for a -10 dB matching with an 8-cell tuner, the Smith chart is almost entirely covered (93.91%). Still the 6-cell tuner provides 87.7% coverage with 1/4th the number of points and can provide a good compromise between coverage and complexity.

2.4.2.2 Coverage versus Frequency
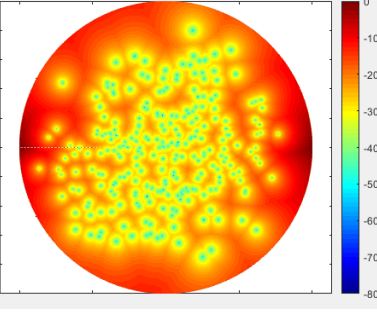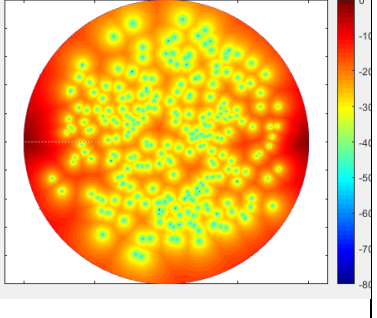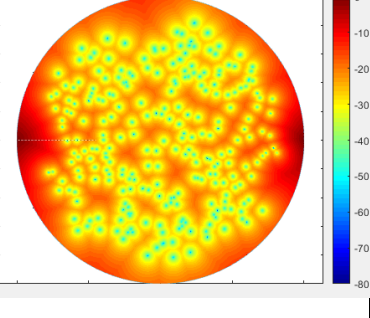
Since the tuner is frequency dependent, in this section we fix all the other parameters, namely the number of cells is fixed at 8, and study the impact of the frequency variation on the tuner coverage. The table 2.3 summarizes the obtained results.

Table 2.3 Coverage in function of the frequency

2 GHz	4 GHz	6 GHz
C-10dB = 61.18 %	C-10dB = 84.07 %	C-10dB = 93.91 %
C-20dB = 38.11 %	C-20dB = 57.61 %	C-20dB = 71.52 %

8 GHz	9 GHz	10 GHz
C-10dB = 97.55%	C-10dB = 97.81 %	C-10dB = 97.85 %
C-20dB = 79.07 %	C-20dB = 84.09 %	C-20dB = 86.01 %

According to table 2.3, the coverage increases sharply between 4 GHz and 6 GHz. For high frequencies, we can notice that the points' distribution becomes better since the points are more distanced. The frequency range depends on the application in which the tuner will be integrated and the matching value needed in the specifications. For example, if the design operates at a low frequency, we have limited impedance values that can be covered. If the design requires a high frequency, we can assume that the tuner design can cover almost all the Smith chart impedances.

As a conclusion, the tuner offers a better reconfigurability when it is integrated in a design that operates at high frequencies but does still offer some coverage for low frequencies.

2.4.2.3 Case Studies

In this section, we study some particular matching cases for a defined frequency. These cases are chosen according to challenging impedance values, which are the impedances quite far from the Smith chart center (50 Ω). The impedances are distributed among the Smith chart's purely resistive, capacitive and inductive regions. Figure 2.12 shows the particular cases identified using ADS simulation.
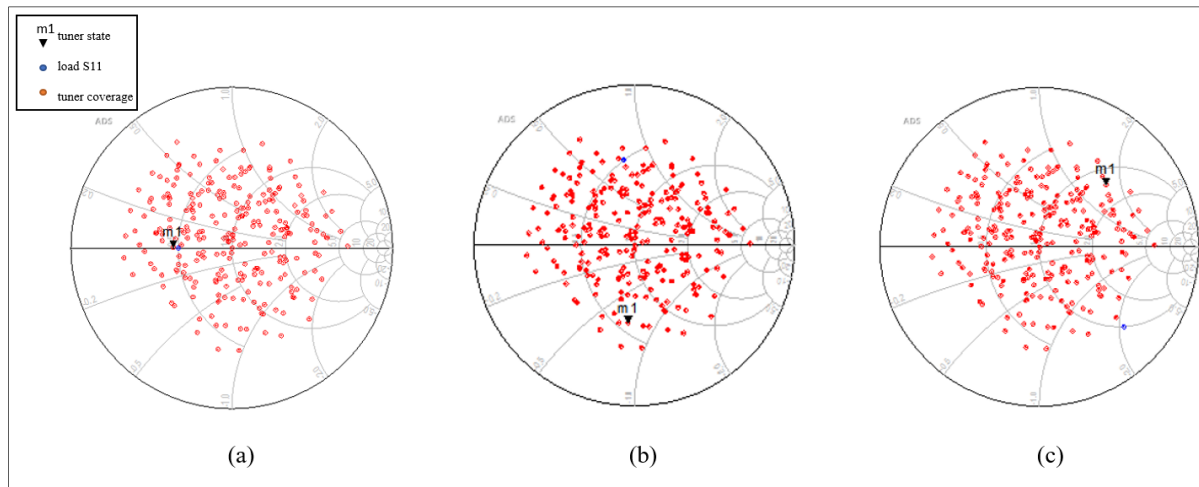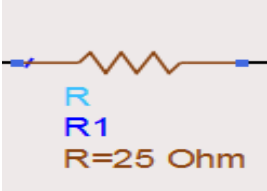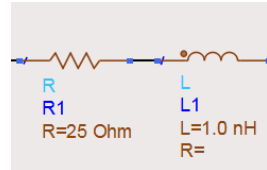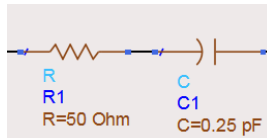
Figure 2.12 (a) a purely resistive, (b) an inductive and (c) a capacitive loads simulated S_{11} superposition to the impedance tuner coverage at 6 GHz

In order to make the parameters more comprehensive we have summarized the results obtained using ADS software in the table below

Table 2.4 Recapitulative of the particular cases simulation result

Load schematic	Impedance to be matched	Impedance tuner settings	Obtained S_{11} (dB)
R R1 R=25 Ohm	$Z = 25\ \Omega$	1110 0111	-15.96
R R1 R=25 Ohm L L1 L=1.0 nH R=	$Z = 25 + j\ 37.7\ \Omega$	0011 0100	-21.62
R R1 R=50 Ohm C C1 C=0.25 pF	$Z = 50 + j\ 106.15\ \Omega$	1100 1010	-32.78

As the tuner shows a good coverage for high frequencies, we can conclude from the table that inductive and capacitive impedances are also covered. However, those values are vulnerable to frequency variation. With the intention of visualising the impact of the frequency variation on S_{11} simulation results, we have chosen a random state (1010 1010) from the previous table and we applied a small frequency variation (From 6 GHz to 8 GHz). The figure 2.12 shows the S_{11} simulated results obtained.
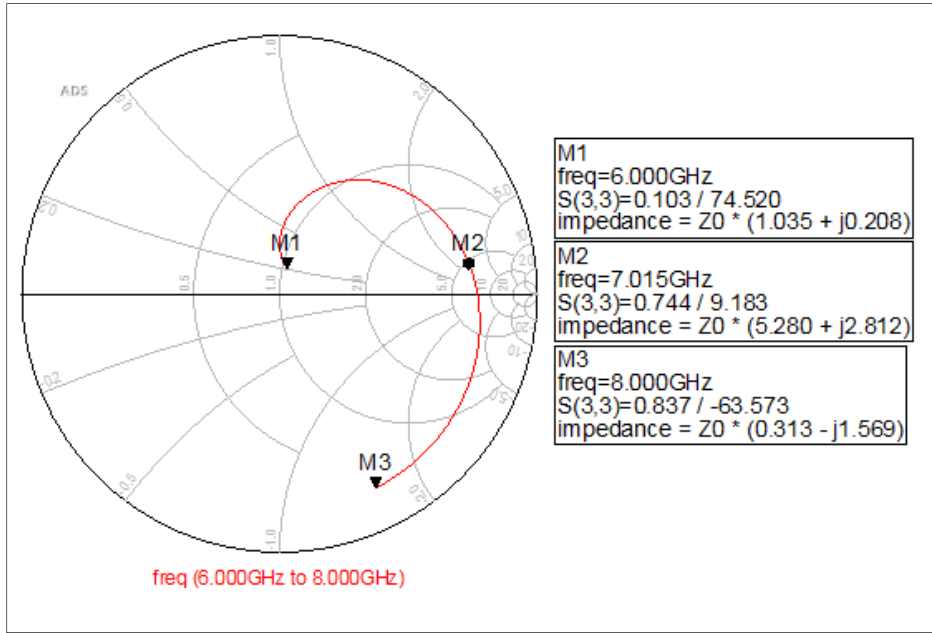
Figure 2.13 Simulated S_{11} for the case 1010 1010 from 6 GHz to 8 GHz

The frequency deviation allows the cell to alter from inductive to capacitive behavior. Thus, the point had moved from almost the Smith chart center to border. From those results, we can conclude that the selection of the tuner state must be precise to fit the device tuning needs. Therefore, having a wide frequency range device will require an alternation between several states from which we can presume the importance of the repeatability of the configuration.

2.4.2.4 Coupling Phenomena

The simulation results presented so far assumed cascaded cells with no interaction between them. Since the cell cavities are separated by a distance of 2 mm, coupling phenomena between the cells may exist and must be investigated. To this end we simulated the entire tuner in HFSS to capture all interactions and coupling phenomena between the cells. We then compared the obtained results to those from cascaded S-parameter files of eight individual cells in ADS

Figure 2.15 shows the superposition of the reflection coefficients and insertion losses for HFSS (blue curve) and ADS (red curve) simulations. The parameters exhibit almost the same behavior indicating the impact of coupling between the cells is minimal.
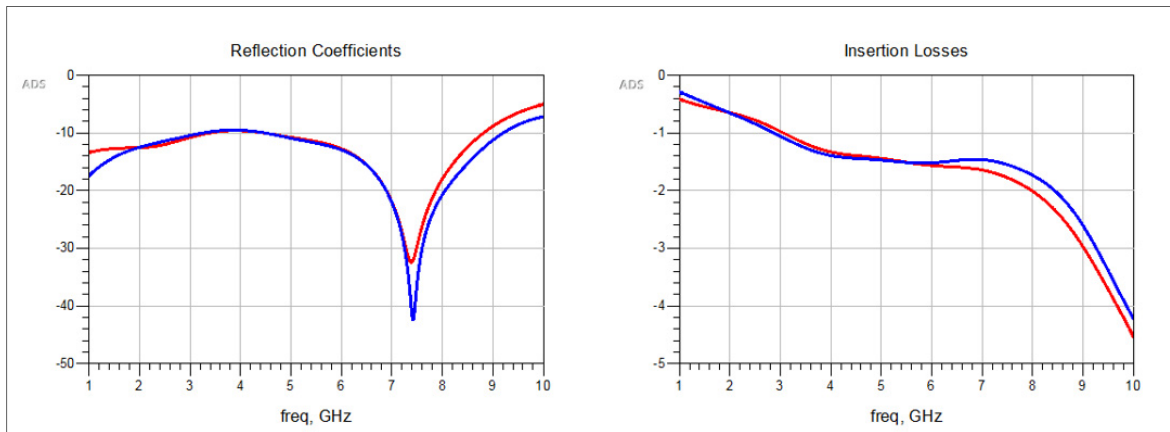
Figure 2.14 HFSS and ADS S-parameters simulations

Figure 2.14 illustrates the electrical field obtained by field simulation for two adjacent LM-filled cavities in the tuner. This figure shows that there is not much coupling between the filled cavities.
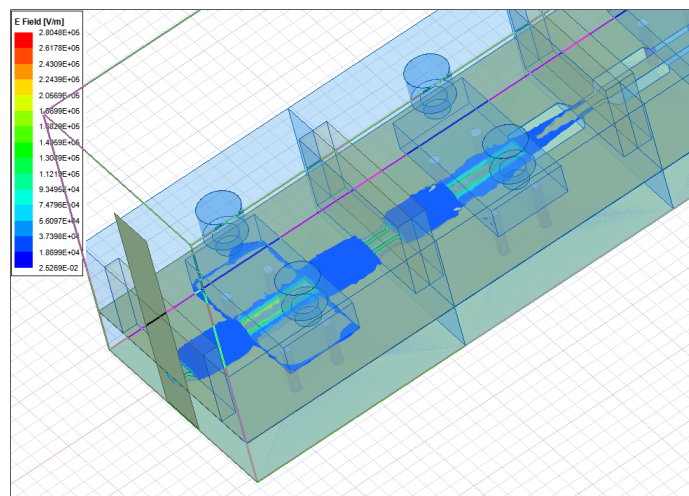
Figure 2.15 Electrical field illustration between two filled cavities

2.5   Conclusion

The design and simulation results for a LM-based reconfigurable impedance tuner were presented. The Smith chart coverage of the tuner versus number of cells and versus frequency were investigated. It was found that tuner's performance in terms of Smith chart coverage increased with frequency and number of cells. For the rest of this thesis an 8-cell design LM-based reconfigurable impedance tuner will be considered.

In the next chapter, we present the details of the design and fabrication of the proposed tuner in LTCC technology. In addition, we explain the steps employed to manipulate the LM and to deal with its injection/extraction challenges.

CHAPITRE 3

FABRICATION AND MEASUREMENT

3.1   Introduction

In this Chapter, we introduce the LTCC technology and describe its fabrication process. Then, we discuss the fabrication of the tuner and highlight the challenges faced. Measured results for the fabricated individual cells and the entire tuner are also presented and compared those obtained by simulation. We conclude this chapter by a repeatability study in which we examine the cavity state after injecting the LM and after removing it.

3.2   LTCC Technology: Generality and Process

The LTCC is a circuit fabrication technology suitable for high volume microwave devices and circuits that must operate under harsh conditions. According to (L.J Golonka 2006), it has been used thanks to its good reliability and stability and the low loss of ceramics at high frequencies. According to (Ingo Wolff 2007), one of the major advantages of the LTCC technologies is the high frequency that can be reached and the ability to integrate diverse circuits in the same structure using different masks as well as the integration of passive components. In addition, it allows the use of different tape materials with different characteristics including ceramic and ferromagnetic materials. The LTCC fabrication process is a multilayer process whereby individual ceramic layers, called ceramic green tape, are first processed by via punching and via filling followed by screen printing of conductive traces. Next, these layer stacked, with precise alignment, pressed into a single laminate, diced and fired. Figure 1.9 summarizes the LTCC fabrication steps. More details on this process are available in LTCC@ETS design guide document (Gravel, N. 2012).
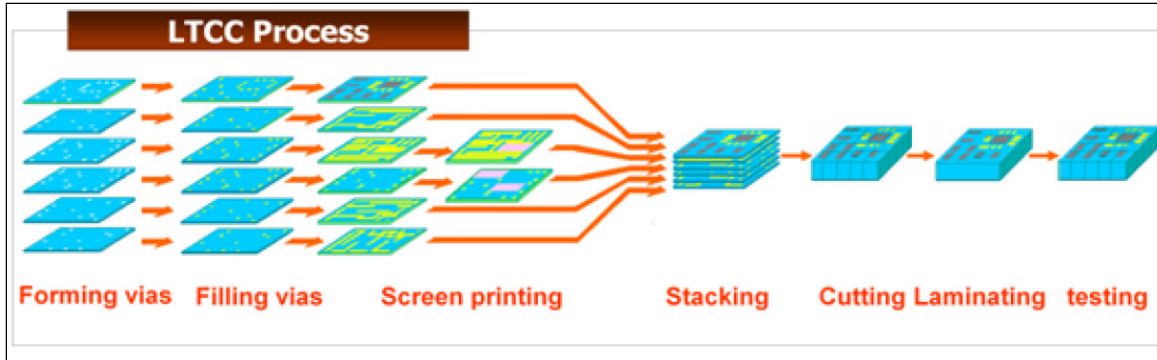
Figure 3.1 LTCC fabrication steps
Taken from LTCC@ETS design guideline

The co-firing step of the LTCC process usually causes shrinkage in the substrate material. Moreover, the shrinkage percentage changes from one material to another and may also vary along x, y and z directions. These values are usually provided by the tape manufacturer and must be taken into account during the design and layout mask generation phases. The LTCC@ÉTS process that we will use for the tuner fabrication is the one based on Dupont's 951 tape with silver metallization. Its shrinkage factors of 12.7% in the x-y plane and 15% in the z-direction.

3.3   Mask Generation

To fabricate the designed cells and tuner, we use the ADS software to prepare and produce the fabrication masks. The design dimensions for all the features and all the layers are captured from the 3D model in ANSYS HFSS. Figure 3.2 shows the superposed multi-layer masks for a single cell. It should be noted that singles cells are measured using the on-wafer technique with a probing station. Therefore, no SMA transitions are added to the single-cell but the input and output GCPW line dimensions are adjusted to be compatible with 100 µm pitch probes.
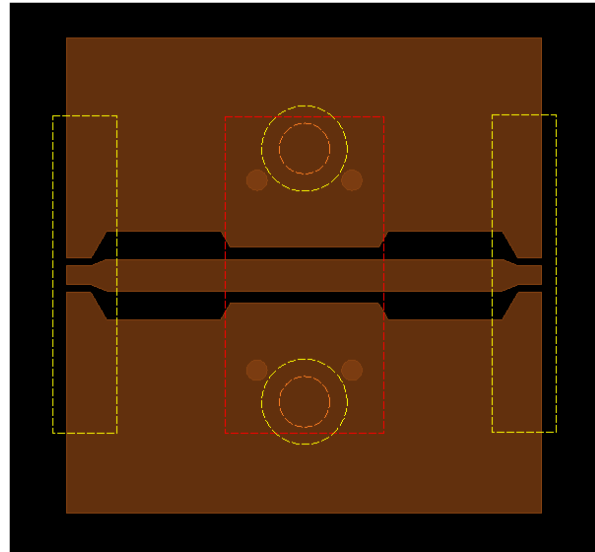
Figure 3.2 Illustration of the cell's layout on the ADS layout

For the mask of the entire tuner, we cascaded eight cells and merged them in into a single layout. As discussed in chapter II, the tuner needs SMA connectors to facilitate LM pumping while measuring its performance. Therefore, we also transferred the DXF file of the designed SMA transition from HFSS to ADS and merged it with the tuner layout at the input and output sides. Figure 3.3 illustrate the tuner's final multilayer mask considering all layers needed for the LTCC fabrication and incorporating the SMA transitions.
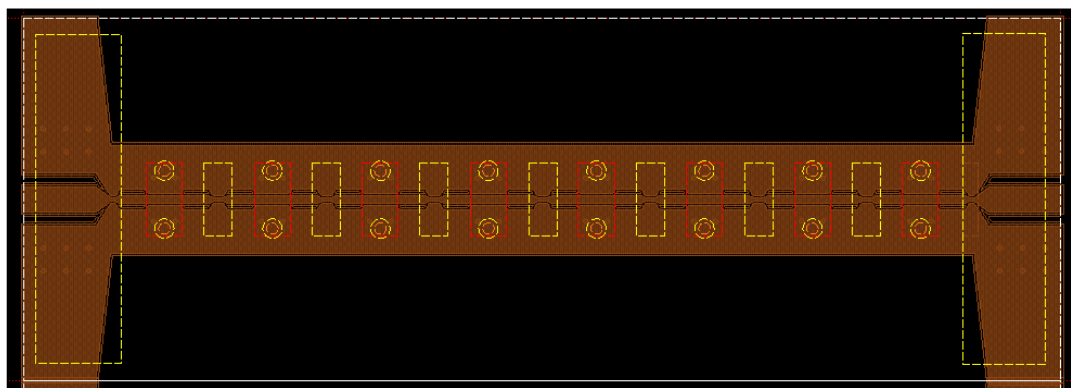
Figure 3.3 Illustration of the tuner's mask in ADS layout

It should be noted that while preparing the layouts for the single cell and the entire tuner, we applied a multiplicative scaling factor to all features on all layers to account for the expected shrinkage during co-firing.

3.4   Fabrication

We start the fabrication using the in-house LTCC technology process discussed in the pervious section. We used eight 5-mil layers of Dupont951 and one 2-mil layer of the same material for the protection layer. The important point in the fabrication is to verify at the end of each step that the results are good before moving to the next step. One of the challenging phases of the LTCC process is metal printing especially that we have small-size features, i.e., the smallest distance between the ground plan of the center line of the GCPW structure is equal to 50 μm. Therefore, after the printing we used a laser ablation operation in order to clean the sheet from the metal residues left between the ground planes and the line, which can cause a short circuit. Figure 3.4 shows a photograph of the printed metal on the third layer. Following each laser ablation operation, we inspect the printed metal again under the microscope and visually inspect its quality. If necessary more ablation steps are carried out until the proper quality is obtained, at which point we move to the next process steps.

(a)   (b)
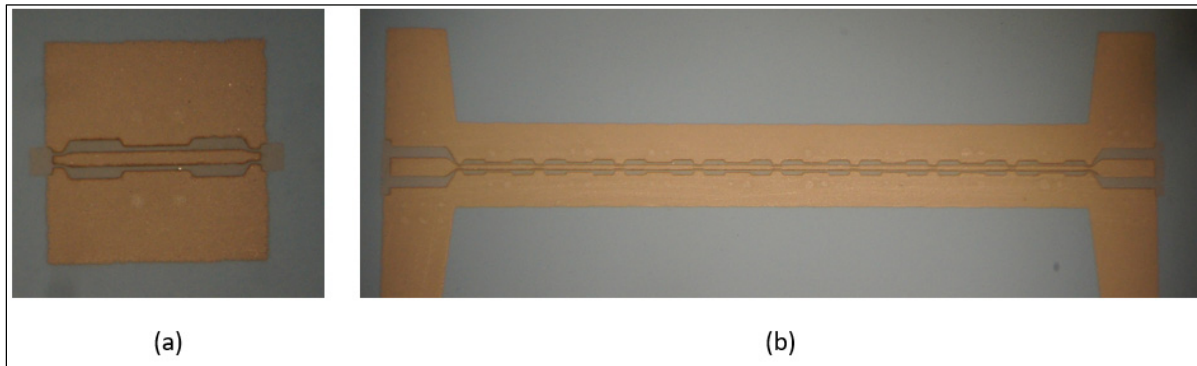
Figure 3.4 Printed metal of (a) the cell and (b) the tuner circuit

The design contains many cavities in each layer. In order to avoid the collapse of these cavities during the lamination step where the LTCC stack is pressed at 270 bar, we have to fill them with fugitive tape after stacking each layer. This carbon-composed fugitive tape ensures mechanical integrity during the pressing step and evaporates during the last step of co-firing.

The alignment of the circuit is also challenging since the circuit requires more accuracy in terms of VIA connections. To ensure the conformity of the alignment, we have checked the VIA connections after stacking the third layer, the layer containing the printed lines, using a multi-meter. In addition, we carried out VIA inspection using an X-ray machine after co-firing. Figure 3.6 shows the result obtained by X-ray imaging for VIAs inspection and confirms good connection between the different layers. Additionally, the continuity of printed lines is verified using both X-rays imaging, particularly for buried traces, and multi-meter measurements in order to make sure that there are no open or short circuits where they are not supposed to be. The results of the X-ray inspection of the entire tuner are shown in figure 3.7 and do not indicate any noticeable fabrication defects.

After verification of the fabricated circuits, we mounted SMA connectors in order to carry out the measurements (figure 3.5).
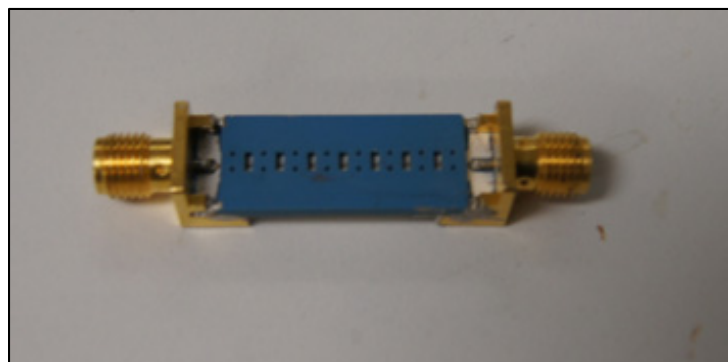
Figure 3.5 Final circuit after SMA connectors insertion
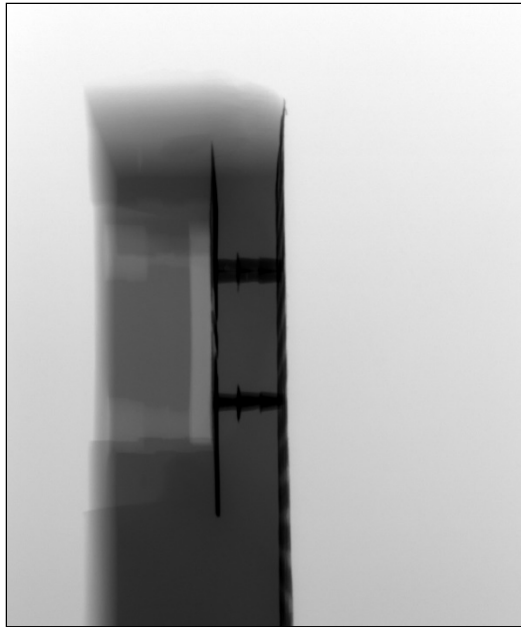
Figure 3.6 VIAs inspection using X-rays machine
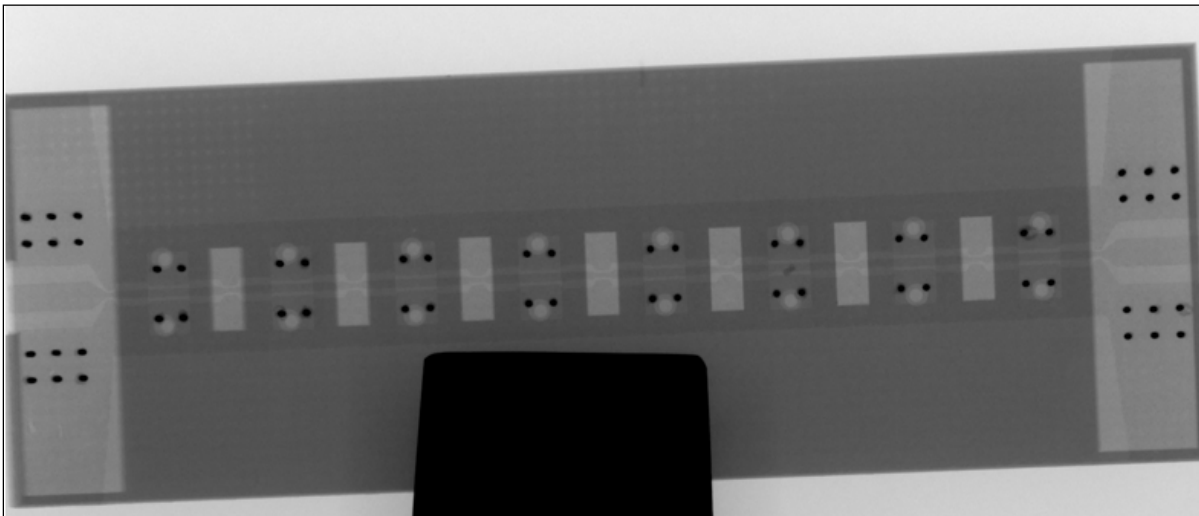
Figure 3.7 The X-rays inspection of the tuner

3.5   Parameter Measurement

First, we measured the S-parameters of the cell in both empty and LM-filled cases and we compared the obtained results to the simulated ones. We then measured the tuner's coverage and S-parameters for the selected states, which were studied in the section 2.4.3 in order to make sure that the coverage can reach as much of the Smith chart as possible.

3.5.1   Liquid Metal Cell Measurements

Using a network analyser and a probing station, we measured the S-parameters for both empty and filled states of the fabricated single cell. Figure 3.8 shows the test bench used for these measurements. The obtained S-parameters measurement results for the empty state are presented in figure 3.9 in blue and are compared the simulated results, shown in red. These results show that matching is good over the entire band and that the simulated and measured insertion loss are in good agreement up to about 9 GHz.
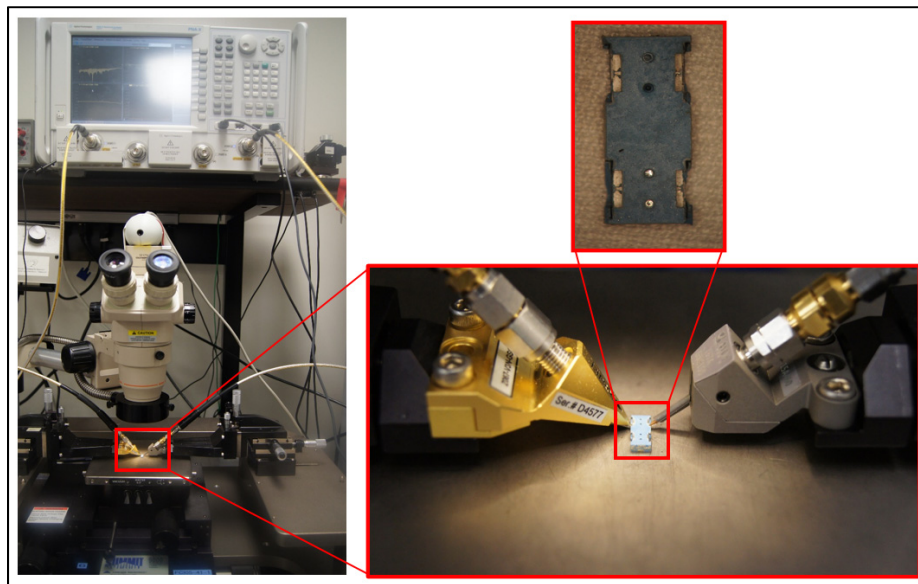
Figure 3.8 Test bench for S-parameters measurement
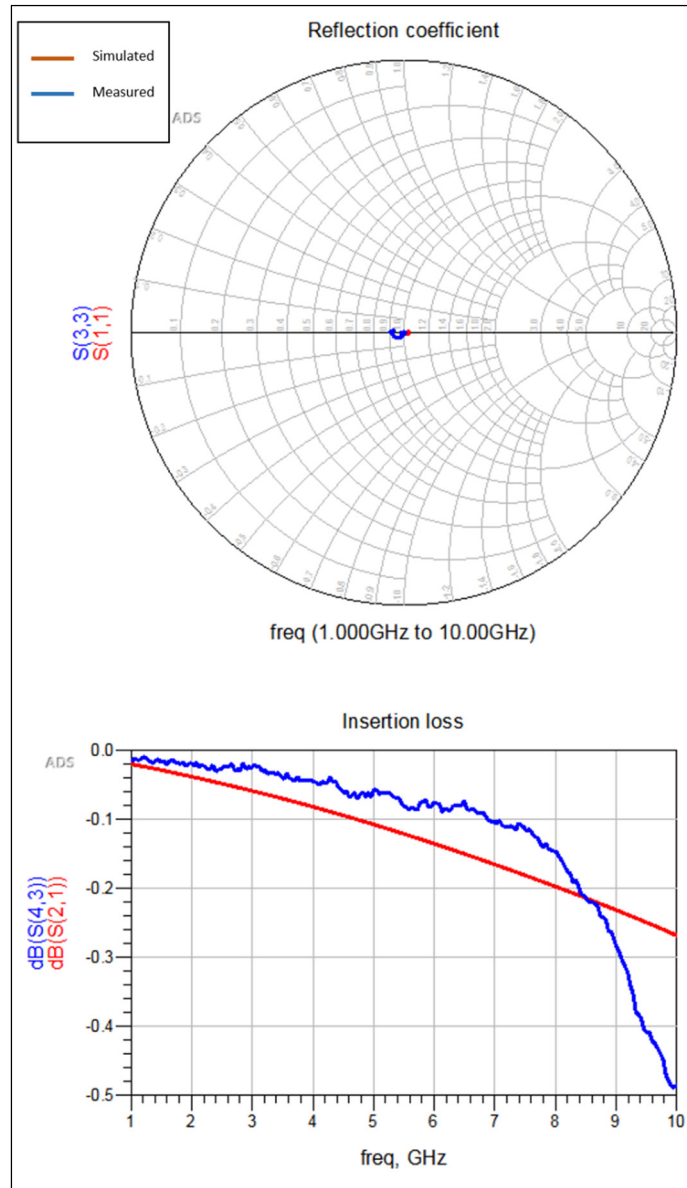
Figure 3.9 Liquid metal cell simulated and measured reflection coefficient
and insertion loss for air-filled cavity

Figure 3.10 shows the simulated (red curves) and measured (blue curves) S_{11} and S_{21} for the
case where the cavity is LM-filled. Once again we observe good agreement between simulated
and measured results over the entire frequency band from 1 to 10 GHz.
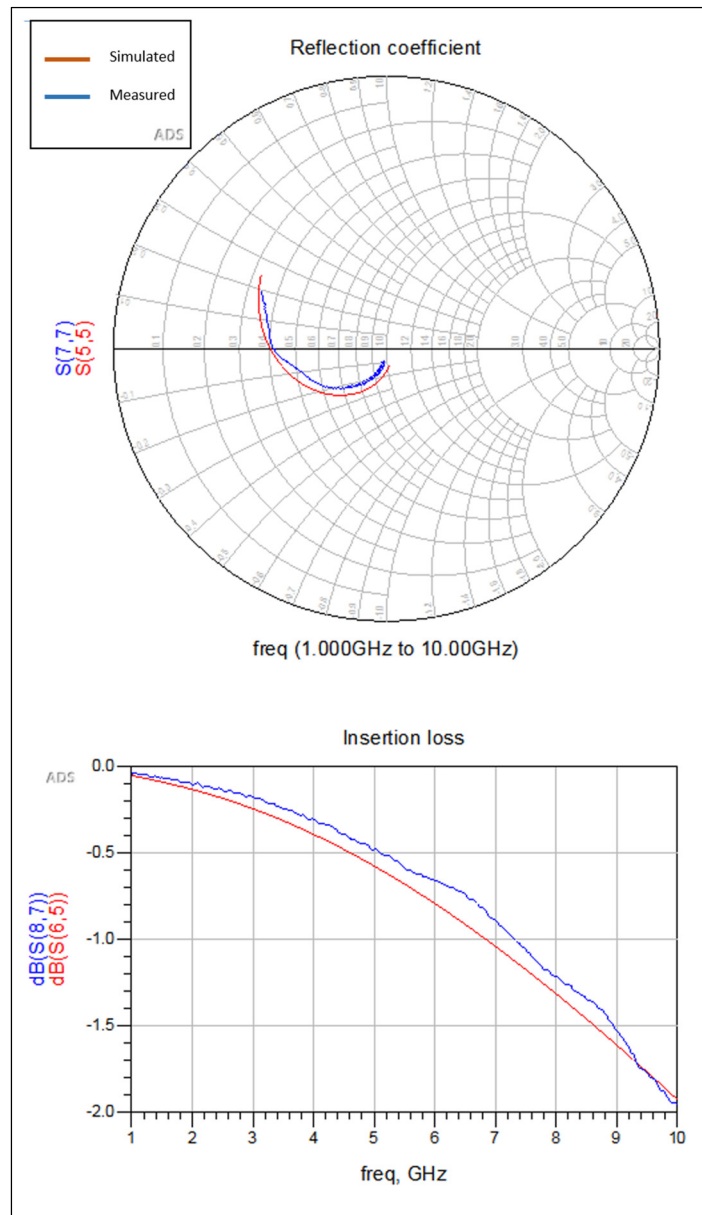
Figure 3.10 Liquid metal cell simulated and measured reflection coefficient
and insertion loss for LM-filled cavity

3.5.2   Liquid Metal Tuner Measurements

3.5.2.1 Coverage Measurement

To obtain the measured S-parameters of the tuner, there is two possible techniques. The first technique (denoted M1) is to connect the tuner to the network analyser and carry out multiple measurements for different tuner states by filling and emptying cavities multiple times. The second method (denoted M2) is based on cascading the single cell's measured S-parameters for both empty and filled states (as discussed in section 3.5.1). This technique, M2, is more adequate in order to predict the anticipated measured performance of the tuner since it allows to easily obtain results for the 256 tuner states as used by (Dorra Bahloul and Ammar B. Kouki, 2020). Figure 3.11 shows the simulated (blue) and M2-measured (red) S_{11} distributions on the Smith chart for the tuner's 256 states 4, 6, 8 and 10 GHz. Next, we calculated coverage percentage for the M2-measred and simulated results using the Matlab code developed to this end. Table 3.1 summarizes the obtained -10dB and -20dB coverage percentage for the simulated and M2-measured results at the four selected frequencies.

Table 3.1 Simulated and M2-measured coverage percentage of the tuner

Frequency (GHz)	Simulated C_{-10dB} (%)	Measured C_{-10db} (%)	Simulated C_{-20db} (%)	Measured C_{-20dB} (%)
4	84.07	76.91	57.51	51.75
6	93.91	92.04	71.52	67.35
8	97.55	95.35	79.07	76.02
10	97.85	96.91	86.01	77.58

Figure 3.11 Simulated and measured S₁₁ distributions for the 256 tuner states

Based on the obtained results, the difference between the simulated and the M2-measured coverage increases slightly with the frequency. As it can be noticed, at 10 GHz, the measured points are more compact compared to the simulated S_{11}, leading a difference in coverage of about 10%. Still, the fabricated tuner coverage is acceptable even at 10 GHz.

3.5.2.2 Measurement of the Empty Tuner

Given the complexity of measuring the entire tuner for all 256 states, we opted for the M2-measurements in the previous section. Here we present the M1-measurements, i.e., entire tuner, but only for the empty tuner state. Unfortunately, the tuner was damaged while pumping the LM because the measurement cables applied torsion on the SMA connectors, which were connected to a thin and fragile transition region. Therefore, we were unable to make M1-measurements for filled states.

Figure 3.12 shows the obtained S_{11} results for the empty state and compares them to simulation and M2-measurements over the entire 1-10 GHz frequency band. It is seen that, although matching is below -10 dB for almost the entire band, there is considerable difference compared to simulations and M2-measurement. This is likely due to the lack of precise repeatability between the tuner cells, i.e., the individual cells are not identical due to process variation, which could amplify frequency dispersion. To examine this more closely, we consider one of the simulated states in the section 2.4.2.3, i.e., the state 1010 1010, and compare the simulated and the measured S_{11} from 6 GHz to 8 GHz as shown in the figure 3.12. The simulated and the measured S_{11} exhibit an overall similar behavior. However, at low frequency the impedance difference in notable and could be due to the difference between simulation and measurement of the SMA connector transitions.
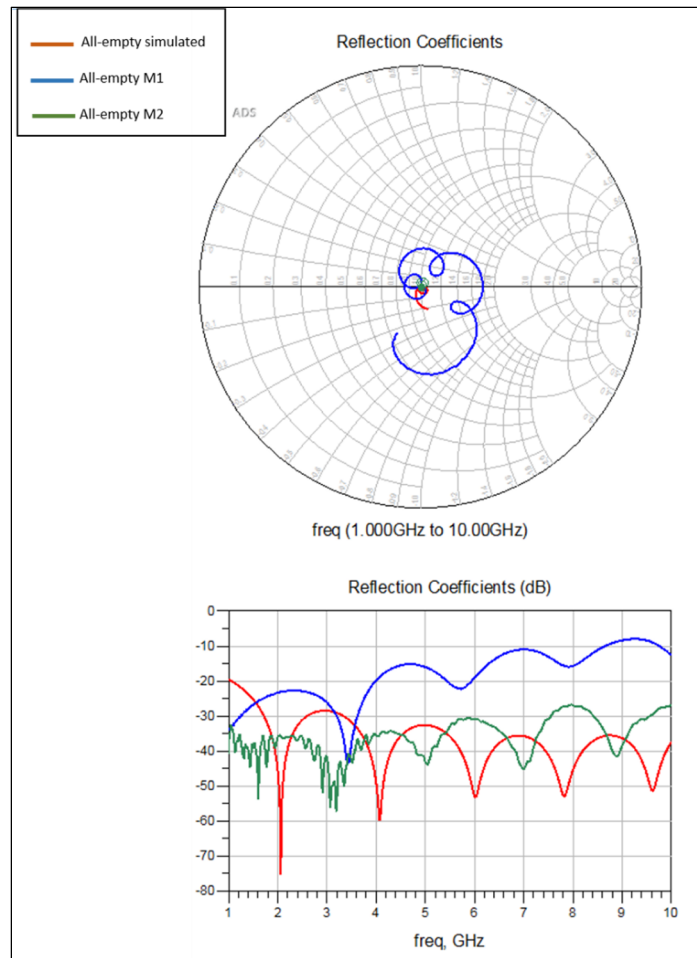
Figure 3.12 The impedance tuner simulated and measured S_{11} at all-empty cavities case
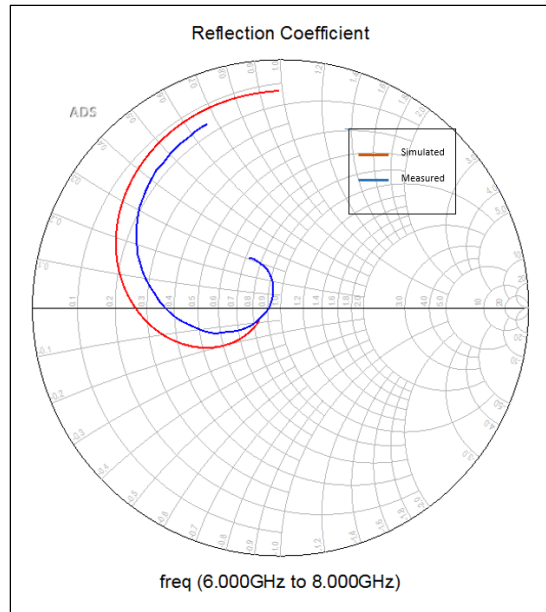
Figure 3.13 LM based tuner simulated and measured S_{11} for
a particular state from 6 GHz to 8 GHz

Figure 3.14 shows compares the simulated and measured S_{21} results for the empty tuner between 1 and 10 GHz. Overall, the agreement is good between simulation and measurements with the M1-measurement showing closer tracking of simulations. The M2-measurement shows better insertion loss than simulation up to around 8.5 GHz and increases rabidly afterwards.
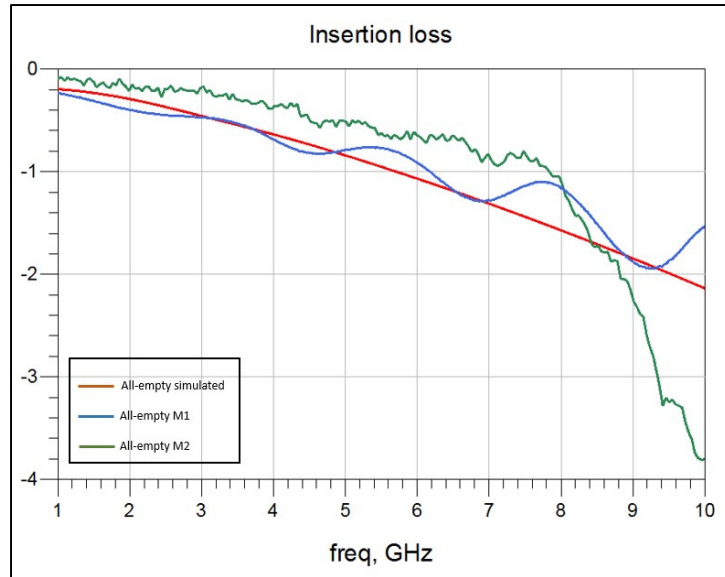
Figure 3.14 Empty cavities tuner simulated and measured insertion loss

3.6   Repeatability study

The tuner reconfigurability is based on two principal operations: the pumping, i.e., filling, of the LM and the cleaning, i.e., emptying, of the cavity. Since the LM oxides quickly, we have done some trials to check if we can return to the initial state after a pumping-cleaning operation. Figure 3.15 shows a photograph under microscope of two side-by-side cells, one empty (left) and one LM-filled (right).
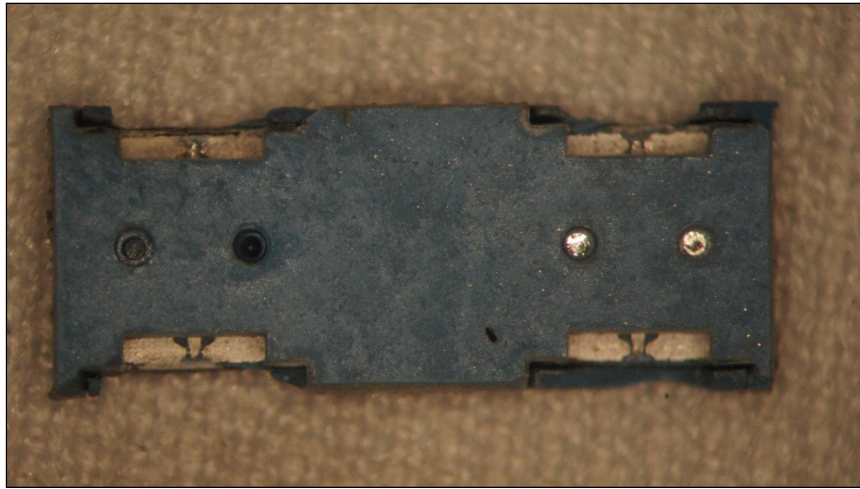
Figure 3.15 Photograph of one empty and one LM-filled cells

3.6.1 Liquid Metal Pumping

The pumping operation is done using a syringe with a needle that fits into cell's outlet. Because of the fast oxidation of the Galinstan we followed the pumping method cited in chapter I (figure 1.8) where an NaOH solution is used during pumping to help prevent the Galinstan from oxidation.

3.6.2 Cavity Cleaning Operation

During regular LTCC fabrication, we often use Isopropyl alcohol, IPA, for circuit cleaning. Therefore, we first investigated its usability LM cleaning. Starting with a LM filled cell, we injected IPA inside its cavity several times to ensure maximum cleaning. Figure 3.16 shows an X-ray image of a reference empty cell and compares it to the IPA-cleaned cavity. As can be noticed, the IPA solution was not efficient in cleaning the cavity and left some residues behind that can influence the tuner's behavior and impact the repeatability of measurements.

Since Galinstan can be easily manipulated using NaOH solution, as a second cleaning option we tried to using a NaOH solution for the cell cleaning in a similar manner to the IPA. Figure

3.17 shows the obtained X-ray images. We can notice that the use of the NaOH solution achieves better cleaning results compared to the IPA as only negligible residues are left inside the cavity.
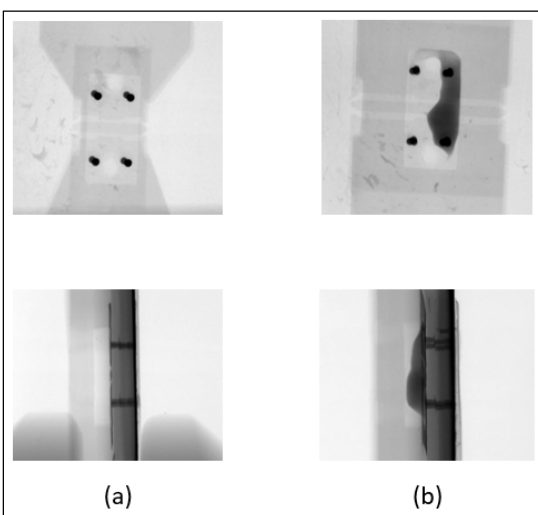
Figure 3.16 X-rays illustration of front and right side views of (a) an empty and (b) a cleaned cells using IPA
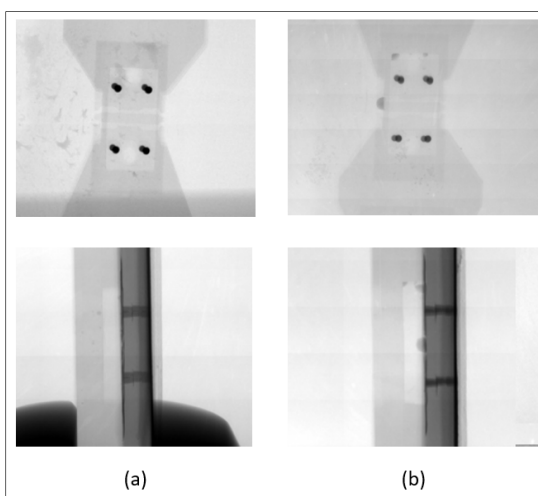
Figure 3.17 X-rays illustration of front and right side views of (a) an empty and (b) a cleaned cells using NaOH

To assess the efficacy of the NaOH cleaning option and determine the repeatability of measurements, we executed the following steps:

- measure the cell's S-parameters at an initial empty state,
- fill the cell's cavity with LM and leave it inside it for 3 days,
- clean the cavity using NaOH solution,
- re-measure the cell's S-parameters after cleaning.

Figure 3.18 shows the obtained results for the reflection coefficient (S_{11}) and insertion loss (S_{21}). These results exhibit a slight shift between the first and second. This can be related to the LM residues left inside the cavity. However, the measurement conditions can also affect the results, since the measurements are not taken at the same time and settings. To conclude, considering the measurements circumstances, the obtained S-parameters shift is tolerable.

.
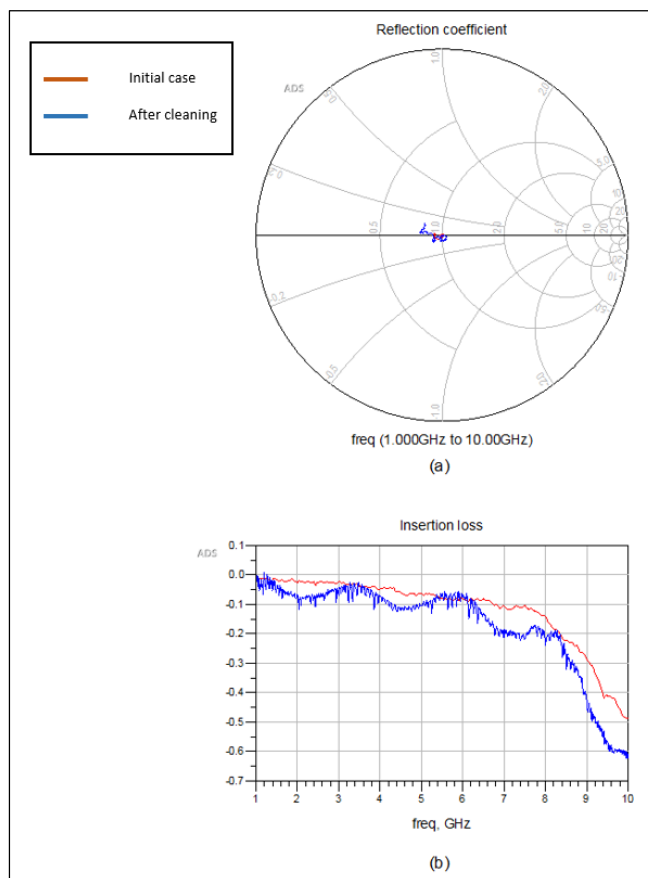
Figure 3.18 Empty cavity-cell measured (a) reflection coefficient and
(b) insertion loss at initial case and after the first cleaning operation

3.7   **Conclusion**

In this chapter, we presented the fabrication of a prototype for a single reconfigurable cell and the entire impedance tuner. We covered several fabrication challenges that require continuous alignment and validation at each step. Then, using a test bench, we measured the fabricated prototypes and compared measured results to simulations and found relatively good agreement that validate the feasibility of desired impedance tuning. We concluded this chapter by a repeatability study in order to determine the LM injection effects on the reconfigurability of the circuit and found that using NaOH good repeatability can be achieved.

The impedance tuner design was one of several RF and microwave applications that employed the LM as it proves a good performance in high frequencies, and it paves the way for innovations. However, LM handling still presents challenges which can undergo more developments that will further facilitate its packaging and manipulation.

CONCLUSION & RECOMMENDATIONS

Fluid-based structures have demonstrated a great potential in various reconfigurable RF and microwave circuits that exploit fluid dielectrics or liquid metals. In the first part of this thesis, a fluidic cell structure was investigated and adapted to operate with liquid metal. The cell structure was design to operate in one of two possible states (air-filled cavity and liquid metal-filled cavity). Based on the single cell design, we developed a liquid metal-based impedance tuner composed of eight cascaded cells. The designed tuner is configured by liquid metal injection that allows it to present 256 possible states.

Further, the cell and the tuner designs were fabricated using LTCC technology with Dupont951 green tape. Several design challenges related to the small-scale dimensions and the various implemented cavities were met and addressed systematically. The fabricated circuits were, then, verified under X-ray imaging and using multi-meter measurements in order to check the continuity and the alignment of the VIA connections.

The fabricated designs were measured, and the results were compared to simulations. The measured coverage reached up to 96.91% for -10 dB matching threshold and 77.58% for -20 dB threshold at 10 GHz. In addition, the insertion loss obtained by tuner's parameters measurements was less than 2 dB. However, the reflection coefficient, when all the tuner's cavities are empty, diverges to -10 dB at the frequency limit (10 GHz). Finally, the repeatability of the liquid metal pumping-removing operation was studied in the final part of this thesis. It was found that using NaOH the measured performance was repeatable after emptying the cavity a very slight degradation in performance. This was due to the negligible LM residues found inside the cavity under X-rays after cleaning.

For future works, this project can be a part of an automated impedance matching network that incorporates measurement and tuner control where the tuner is placed between an unmatched device and the measurement system and controller searches for the optimal tuner setting to achieve best matching in near-real time. The measurement can be accomplished using the

embedded vector measurement of RF/Microwave circuits in LTCC technology proposed in (Mohamed, H. 2019). A microcontroller based platform can be used to interface to the measurement system and to control micro pumps that fill/empty the proper tuner cavities.

Additional improvements to the tuner design should also be considered to make it more mechanically robust, particularly at the SMA connector locations. Further investigation into the repeatability of the filling emptying operations and the speed at which they can be accomplished with minimum impact on performance should also be considered. Finally, this work can be extended to applications such as antenna tuning and implementation of reconfigurable intelligent surfaces (RIS) which have been recently introduced for future 6G systems.

ANNEX I

DESIGN MODEL

$$\varepsilon_{eff} = 1 + \frac{(\varepsilon_r - 1)\left(\frac{K(K_1)}{K(K'_1)} + \frac{K(K_2)}{K(K'_2)}\right) + (\varepsilon_{up} - \varepsilon_r)\frac{K(K_c)}{K(K'_c)}}{\frac{K(K_3)}{K(K'_3)} + \frac{K(K)}{K(K')}} \tag{2.2}$$

$$Z_0 = \frac{60\pi}{\sqrt{\varepsilon_{eff}\left(\frac{K(K_3)}{K(K'_3)} + \frac{K(K)}{K(K')}\right)}} \tag{2.3}$$

$$\varepsilon_{up} = \begin{cases} \varepsilon_r & for \quad S2 \quad and \quad S4 \\ \varepsilon_c & for \quad S3 \end{cases} \tag{2.4}$$

$$K = \frac{W}{W + 2.G} \tag{2.5}$$

$$K_I = \frac{\sinh\left[\pi.\frac{W}{4.h_i}\right]}{\sinh\left[\pi.\frac{(W + 2.G)}{4.h_i}\right]} \quad ; i = \{1, 2, c\} \tag{2.6}$$

$$K_3 = \frac{\tanh\left[\pi.\frac{W}{4.h_1}\right]}{\tanh\left[\pi.\frac{(W + 2.G)}{4.h_1}\right]} \tag{2.7}$$

$$K'_i = \sqrt{1 - K_i^2}; i = \{1, 2, 3, c\} \tag{2.8}$$

LIST OF BIBLIOGRAPHICAL REFERENCES

Bahloul, D., Kouki, A. B. (2020). LTCC-Based Fluidic Tuners for Low Microwave Frequency Reconfigurable Circuits. IEEE Transactions on Microwave Theory and Techniques, 68(8), 3308–3317.

Boeck, G., Plenkowski, D., Circa, R., Otte, M., Heyne, B., Rykaczewski, P., Wittmann, R., & Kakerow, R. (2003). RF front-end technology for reconfigurable mobile systems. Proceedings of the 2003 SBMO/IEEE MTT-S International Microwave and Optoelectronics Conference - IMOC 2003. (Cat. No.03TH8678), 2, 863–868 vol.2.

Boles, T., Brogle, J., Hoag, D., & Curcio, D. (2011). AlGaAs PIN diode multi-octave, mmW switches. 2011 IEEE International Conference on Microwaves, Communications, Antennas and Electronic Systems (COMCAS 2011), 1–5.

Gravel, N. (2012), LTCC design guideline

K. Buisman', L.C.N. de Vreede', L.E. Larson2, M. Spirito', A. Akhnoukh', Y. Lin', X. Liu', and L.K. Nanver (2005). Low-Distortion, Low-Loss Varactor-Based Adaptive Matching Networks, Implemented in a Silicon-on-Glass Technology. IEEE Radio Frequency integrated Circuits (RFIC) Symposium, 4–7.

Cheng, S., & Wu, Z. (2012). Microfluidic electronics. Lab on a Chip, 12(16), 2782.

David M. Pozar (2012). Microwave Engineering. John Wiley & Sons.

Dominigue, F., Fouladi, S., Mansour, R. (2010), A Reconfigurable Impedance Matching Network Using Dual-Beam MEMS Switches for an Extended Operating Frequency Range, IEEE/Anaheim, CA, USA.

Domingue, F. (2008). RÉSEAUX D'ADAPTATION D'IMPEDANCE AJUSTABLES A BASE DE COMPOSANTES MEMS RF POUR LES APPLICATIONS BASSES FRÉQUENCES. 182.

Elassy, K. S., Rahman, M. A., Yama, N. S., Shiroma, W. A., & Ohta, A. T. (2019). Complex Permittivity of NaOH Solutions Used in Liquid-Metal Circuits. IEEE Access, 7, 150150–150156.

Fouladi, S., Domingue, F., & Mansour, R. (2012). CMOS-MEMS tuning and impedance matching circuits for reconfigurable RF front-ends. 2012 IEEE/MTT-S International Microwave Symposium Digest, 1–3.

Gaevski, M., Deng, J., Gaska, R., Shur, M., & Simin, G. (2014). GaN microwave varactors with insulated electrodes. Physica Status Solidi c, 11(3–4), 853–856.

Golonka, L. J. (2006). Technology and applications of Low Temperature Cofired Ceramic (LTCC) based sensors and microsystems. 11.

Gough, R. C., Morishita, A. M., Dang, J. H., Hu, W., Shiroma, W. A., & Ohta, A. T. (2014). Continuous Electrowetting of Non-toxic Liquid Metal for RF Applications. IEEE Access, 2, 874–882.

Grove, T. T., Masters, M. F., & Miers, R. E. (2005). Determining dielectric constants using a parallel plate capacitor. American Journal of Physics, 73(1), 52–56.

Khondoker, M. A. H., & Sameoto, D. (2016). Fabrication methods and applications of microstructured gallium based liquid metal alloys. Smart Materials and Structures, 25(9), 093001.

Kim, D., Lee, Y., Lee, D.-W., Choi, W., Yoo, K., & Lee, J.-B. (JB). (2015). Hydrochloric acid-impregnated paper for gallium-based liquid metal microfluidics. Sensors and Actuators B: Chemical, 207, 199–205.

Kim, D., Lee, Y., Lee, D.-W., Choi, W., & Lee, J.-B. J. B. (2013). Hydrochloric acid-impregnated paper for liquid metal microfluidics. 2013 Transducers Eurosensors XXVII: The 17th International Conference on Solid-State Sensors, Actuators and Microsystems (TRANSDUCERS EUROSENSORS XXVII), 2620–2623.

Koo, C., LeBlanc, B. E., Kelley, M., Fitzgerald, H. E., Huff, G. H., & Han, A. (2015). Manipulating Liquid Metal Droplets in Microfluidic Channels with Minimized Skin Residues toward Tunable RF Applications. Journal of Microelectromechanical Systems, 24(4), 1069–1076.

Lei, B. J., Hu, W., Ohta, A. T., & Shiroma, W. A. (2012). A liquid-metal reconfigurable double-stub tuner. 2012 IEEE/MTT-S International Microwave Symposium Digest, 1–3.

Liu, T., Sen, P., & Kim, C.-J. (2012). Characterization of Nontoxic Liquid-Metal Alloy Galinstan for Applications in Microdevices. Journal of Microelectromechanical Systems, 21(2), 443–450.

Mohamed, H. (2019). Embedded Vector Measurement of RF/Microwave Circuits in LTCC Technology. 101.

Moorefield, M. R., Gough, R. C., Ohta, A. T., & Shiroma, W. A. (2018). An Electrically Actuated DC-to-11-GHz Liquid-Metal Switch. IEEE Access, 6, 1261–1266.

Morishita, A. M., Dang, J. H., Gough, R. C., Ohta, A. T., & Shiroma, W. A. (2015). A tunable amplifier using reconfigurable liquid-metal double-stub tuners. 2015 Texas Symposium on Wireless and Microwave Circuits and Systems (WMCS), 1–4.

Nemati, H. M., Fager, C., Gustavsson, U., Jos, R., & Zirath, H. (2009). Design of Varactor-Based Tunable Matching Networks for Dynamic Load Modulation of High Power Amplifiers. IEEE Transactions on Microwave Theory and Techniques, 57(5), 1110–1118.

Nikolaou, S., Bairavasubramanian, R., Lugo, C., Carrasquillo, I., Thompson, D. C., Ponchak, G. E., Papapolymerou, J., & Tentzeris, M. M. (2006). Pattern and frequency reconfigurable annular slot antenna using pin diodes. *IEEE Transactions on Antennas and Propagation*, *54*(2), 439–448.

Rebeiz, G. M. (2004). RF MEMS: Theory, Design, and Technology. John Wiley & Sons.

Vähä-Heikkilä, T., Caekenberghe, K. V., Varis, J., Tuovinen, J., & Rebeiz, G. M. (2007). RF MEMS impedance tuners for 6–24 GHz applications. International Journal of RF and Microwave Computer-Aided Engineering, 17(3), 265–278.

Whatley, R. B., Zhou, Z., & Melde, K. L. (2006). Reconfigurable RF impedance tuner for match control in broadband wireless devices. IEEE Transactions on Antennas and Propagation, 54(2), 470–478.

Wolff, I. (2007). Design and Technology of Microwave and Millimeterwave LTCC Circuits and Systems. 2007 International Symposium on Signals, Systems and Electronics, 505–512.

Zhu, L., Wang, B., Handschuh-Wang, S., & Zhou, X. (2020). Liquid Metal–Based Soft Microfluidics. Small, 16(9), 1903841.